Annals of Biomedical Engineering, Vol. 37, No. 11, November 2009 (© 2009) pp. 2337–2359
DOI: 10.1007/s10439-009-9779-x

Development and Validation of a Predictive Bone Fracture Risk Model for Astronauts

EMILY S. NELSON,[1] BETH LEWANDOWSKI,[1] ANGELO LICATA,[3] and JERRY G. MYERS[2]

[1]Bioscience and Technology Branch, NASA Glenn Research Center, M/S 110-3, Cleveland, OH 44135, USA; [2]Human Research Program, NASA Glenn Research Center, Cleveland, OH 44135, USA; and [3]Cleveland Clinic, Cleveland, OH, USA

(*Received 30 April 2009; accepted 4 August 2009; published online 26 August 2009*)

Abstract—There are still many unknowns in the physiological response of human beings to space, but compelling evidence indicates that accelerated bone loss will be a consequence of long-duration spaceflight. Lacking phenomenological data on fracture risk in space, we have developed a predictive tool based on biomechanical and bone loading models at any gravitational level of interest. The tool is a statistical model that forecasts fracture risk, bounds the associated uncertainties, and performs sensitivity analysis. In this paper, we focused on events that represent severe consequences for an exploration mission, specifically that of spinal fracture resulting from a routine task (lifting a heavy object up to 60 kg), or a spinal, femoral or wrist fracture due to an accidental fall or an intentional jump from 1 to 2 m. We validated the biomechanical and bone fracture models against terrestrial studies of ground reaction forces, skeletal loading, fracture risk, and fracture incidence. Finally, we predicted fracture risk associated with reference missions to the moon and Mars that represented crew activities on the surface. Fracture was much more likely on Mars due to compromised bone integrity. No statistically significant gender-dependent differences emerged. Wrist fracture was the most likely type of fracture, followed by spinal and hip fracture.

Keywords—Monte Carlo method, Probabilistic modeling, Biomechanical model, Risk assessment, Fracture risk index, Lumbar spine, Femoral neck, Wrist, Gravitational physiology, Bone loss.

NOMENCLATURE

ABBREVIATIONS

AL	Applied load (N)
BFxRM	Bone fracture risk model
BM	Body mass (kg)
BMC	Bone mineral content (g/cm^3)
BMD	Bone mineral density (g/cm^2)
CoM	Center of mass
DXA	Dual energy X-ray absorptiometry, a means of quantifying BMD
EVA	Extra-vehicular activity
F	Female
FL	Fracture load (N)
FN	Femoral neck
FOR	Factor of risk
FRI	Fracture risk index
LS	Lumbar spine
LSAH	Longitudinal Study of Astronaut Health
M	Male
n	Sample size
p	Probability
QCT	Quantitative computed tomography, a means of quantifying BMC

Variables

a	A general empirical coefficient
b	Damping coefficient (kN s/m)
F	Force (N)
h	Height (cm)
k	Stiffness coefficient (kN/m)
l	Length (cm)
m	Mass (kg)
x	Displacement (cm)
VO_{2max}	O_2 capacity during maximum aerobic exercise (mL/(kg min))
β	Posterolateral angle of impact (°)
ϕ	Slope factor
μ	Position factor
σ	Standard deviation
θ	Trunk flexion angle (°)

Subscripts

a	Active response
A	Arm

Address correspondence to Emily S. Nelson, Bioscience and Technology Branch, NASA Glenn Research Center, M/S 110-3, Cleveland, OH 44135, USA. Electronic mail: Emily.S.Nelson@grc.nasa.gov

BL	Bone loss
CM	Center of mass of the torso
e	Earth
eff	Effective
F	Feet
G	Ground
GR	Ground reaction (force)
H	Hip
HAT	Head, arms and torso
LS	Lumbar spine
O	Object
PL	Pelvis and legs
PM	Postural muscles
s	Suit
S	Shoulder
T	Torso
tot	Total body
UB	Upper body
W	Wrist
Wa	Waist
WaS	Waist to shoulder

INTRODUCTION

This paper describes the development and validation of a physics-based model to predict the risk of bone fracture for astronauts based on skeletal loading. As a group, astronauts are well-conditioned and athletic.[92] It is clear that the duration of time in space is correlated to significant bone loss.[68,115] As a result, there is a legitimate concern that the bones of an astronaut on extended space missions will be less resistant to fracture. Without access to emergency room care, a fracture could have catastrophic consequences for the crew and for the mission. We have developed a tool to assess the risk of bone fracture during routine activities such as lifting, as well as accidents due to falls from moderate height, taking into account the effects of spaceflight and the local gravitational acceleration.

In developing the model, we have focused our attention on regions that are at particular risk, including the femoral neck (FN), the wrist and the lumbar spine (LS).[119] An examination of the literature shows that a broad range of fracture complications occur due to a fall from height, but many studies identify the spine as a common fracture location.[28,32,94,107] The risk of spinal fracture is real, even at falls from moderate heights,[47,98,111,129,134,136] especially for falls onto hard surfaces.[66,94,136] The FN is at risk during a fall to the side,[108] particularly in the case of posterolateral impact.[14,43,60,122] In some cases, the faller can respond actively by extending an arm to absorb some of the impact, which can then put the wrist in danger of fracture.[20,53] In addition to modeling likely scenarios for accidents during a space mission, we included the risk of fracture resulting from lifting a heavy object, which represents a danger for those with substantially reduced bone density,[90] and is also a routine and common task that is essential to mission operations. In this paper, we will describe the resulting set of biomechanical models that mathematically characterize the forces created during a static lift, a fall or jump from the Lunar Lander (or similar) ladder, and a fall to the side during an Extra-Vehicular Activity (EVA). We then use bone fracture models to predict the load at which a particular bone would fracture. Finally, we compare the applied load and the bone strength to ascertain if conditions exist such that a fracture could occur. For the particular case of astronauts, we use pre-mission bone density as a basis on which calculate the cumulative bone loss due to time spent in space over the course of a mission.

Aside from this deterministic infrastructure, parameters such as bone density, weight, gender, and details of the fall are associated with statistical distributions that describe the envelope of possibility. In the case of astronaut falls, the model uses data gathered from the Apollo program to forecast the likelihood of a fall during an EVA. Other parameters include the height of a fall, the likelihood of active response, tissue stiffness and damping, the amount of padding in the spacesuit at the hip, and the weight of an object used in a static lift. This approach also yields a sensitivity analysis, which ranks the parameters in terms of their importance in determining fracture risk.

Since there is no data available for validation of actual space scenarios, we tested the model against terrestrial studies of bone fracture. We adapted the model to match any specified statistical variation in the population of interest, including weight, age, gender, measures of bone health, and heights of falls.

We will first describe the model itself, followed by a discussion of the validation studies. We then extend the model to predict fracture likelihood on lunar and Martian reference missions.

DESCRIPTION OF THE ASTRONAUT BONE FRACTURE RISK MODEL (BFXRM)

We developed a bone fracture analysis tool, the bone fracture risk model (BFxRM), to estimate bone fracture probability and incidence rates for long-duration space missions. The computational model described below is combined with biomedical research and clinically observed data to establish a framework for addressing fracture risk scenarios due to falls, side impacts, drop landings and lifting. The BFxRM takes

into account specific crew data, such as age, height, body mass, pre-flight bone mineral density (BMD), the cumulative low-gravity exposure, impact energy absorption and dispersion capabilities of the EVA suit, active protective response, as well as specific mission profiles and astronaut tasks that lead to high levels of skeletal loading. The conceptual framework of the BFxRM is illustrated in Fig. 1. Mission parameters specify the envelope of tasks and accidents, gravitational environments and the anatomical and physiological characteristics that the simulation will consider. An initiating event triggers a calculation of the forces applied to the skeletal location of interest, followed by an estimate of the current bone strength. We then compare the applied load (AL) to the fracture load (FL) to determine whether or not fracture could occur.

The simulation takes place within the context of well-established probabilistic risk analysis. Many contributing factors in the models discussed here exhibit high variability and uncertainty. This model provides for uncertainties due to known population variation (aleatory), as well as for uncertainties due to lack of knowledge (epistemic). Statistical distributions are established to represent each varying parameter, including subject variation (such as weight and BMD) and event variation (such as height of fall or weight lifted). Our approach estimates the probability of fracture through a Monte Carlo procedure in a statistically based analysis that tests many thousands of combinations of the contributing factors. It then pools the results to yield a quantified fracture probability, described by a mean and standard deviation. The results also identify the factors that most influence the predicted uncertainty through small variations. These measures can supply mission planners with improved decision-making confidence by providing a familiar metric (i.e., the probability of occurrence) for an unfamiliar situation.

Two rules form the philosophy behind the BFxRM modeling approach:

1. *Keep it simple*. Calculations within the model framework must be accurate, but are reduced to the simplest possible form to minimize computational burden.
2. *Use the best, most comprehensive data available*. We developed the model parameters using the most up-to-date, well-accepted and statistically significant data to reduce the overall model uncertainty in the forecasted outcome.

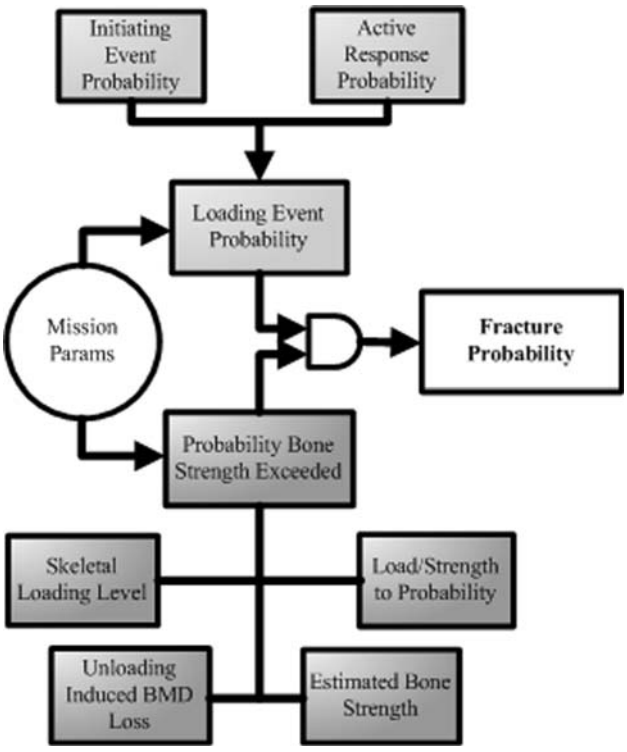

FIGURE 1. Conceptual outline of the bone fracture risk model (BFxRM). The model is split into two sections, the first dealing with the initiating event (generally extra-skeletal factors) and the second addressing biomechanical aspects of the event (generally intra-skeletal factors). Probabilities from both contributors are used to calculate the fracture probability.

Estimation of Bone Strength

Many calculations within the probabilistic model depend on knowing certain physical parameters of the astronaut subjects, such as body mass and the pre-flight bone mineral density at the skeletal location of interest. Flight-ready astronauts are significantly more healthy and fit than the general population.[92] Their pre-flight aerobic capacity must be at or above the mean value for their age, as set by the American College of Sports Medicine Guidelines.[92] At the average age of 45 ± 5 years,[91] astronauts are required to have a $VO_{2max} \geq 38.1$ mL/(kg min) for men and $VO_{2max} \geq 30.9$ mL/(kg min) for women, prior to flight.[92] They must have healthy bone mass with a pre-flight t-score of -1 or better. Similarly high standards are placed on muscular strength and sensorimotor, muscular, hematological and immunological function.[92] We therefore consider the astronaut cohort as a highly targeted population with parameter variations independent of those of the general population. Wherever possible, we develop astronaut parameters directly from the NASA Longitudinal Study of Astronaut Health (LSAH), e.g., body mass.[91] If such data is not available, then the parameters are based on the most relevant populations that can be found, such as athletes and military personnel. We parameterize gender, initial BMD, and mission day of occurrence as

inputs to the bone fracture risk model to characterize the bone mass at the time of fracture.

During each trial of the Monte Carlo simulation, we determined a body mass by randomly sampling a normal distribution with mean and standard deviation of 85.15 ± 0.13 kg for men, and 60.73 ± 8.25 kg for women. To prevent unrealistic values of body mass, we set range limits between 50 and 114 kg. For initial BMD, we used US population data from the NHANES III study, which provided gender- and race-specific values by decade of life.[99] We erred on the conservative side by using data for white Americans, since African-Americans tend to have higher BMD. Based on the data for 45 year-old white Americans, the pre-flight BMD used in this model was 1.002 ± 0.140 g/cm^2 for men, and 0.920 ± 0.136 g/cm^2 for women.

In this study, we will examine several reference space missions as specified in Table 1. The local gravitational accelerations are used in the calculation of body weight and impact velocity. During space travel, the astronauts are subjected to (nearly) zero gravity, and the gravity levels on the lunar and Martian surfaces are approximately 1/6th and 3/8th of the value at the earth's surface, $g_e = 9.8$ m/s^2.

The unloading of the skeletal system (due to the near-removal of gravitational forces in space and other physiological changes) result in site-specific loss of bone mass during the time spent in microgravity. The NASA Fitness for Duty Standards[92] require that astronauts have a hip BMD t-score of not less than -1 (or BMD > 0.820). (The t-score represents an individual's BMD by the number of standard deviations from the mean BMD of an applicable reference race, gender and age population. In this case 0.942 ± 0.122 g/cm^2 is used.) The goal is to ensure that the post-flight t-score will be -2 or better (or BMD > 0.698). LeBlanc *et al.*[67] performed the seminal study documenting areal BMD loss rates in space. They evaluated experimental pre- and post-flight measurements of BMD using dual energy X-ray absorptiometry (DXA) on 18 cosmonauts with missions ranging from 4 to 14 months in duration. For the hip and lumbar spine, the percentage loss in BMD per month in space was slightly more than 1% of the initial value (femoral neck: 1.06 ± 0.63%; trochanter: 1.56 ± 0.99%; lumbar spine: 1.06 ± 0.63%).

TABLE 1. Definition of mission scenarios.

Mission reference	Gravity (m/s^2)	Outbound transit time (days)	Duration of stay (days)	Return to earth (days)
Lunar short	1.62	3	8	3
Lunar long	1.62	5	170	5
Mars short	3.71	162	40	162
Mars long	3.71	189	540	189

Other parts of the body, such as the arm, are reduced in BMD to a lesser degree (arm: 0.04 ± 0.88%). In the BFxRM, we assumed a linear decrease of BMD with time in space, since the data were based on estimates obtained strictly from these (two-point) pre-flight and post-flight measures to yield $\mathrm{BMD}(t) = \mathrm{BMD}(1 - a_{\mathrm{BL}}t/30)$, where $a_{\mathrm{BL}} = 1.06 \pm 0.63$ and time t is measured in days.

There is as yet no data to confirm that the pattern of bone loss is linear over long time spans, nor that it continues unabated throughout a planned long-duration mission. However, there is some terrestrial evidence that bone mass may plateau after a period of significant loss. A review of bone loss in one of the most significant disuse medical conditions, spinal cord injuries (SCI), indicates that after a peak rate of bone loss at 3–5 months post-injury, the bone metabolic process tends toward steady state after 16–24 months, with BMD loss rates approaching those normally seen with increasing age (see the review by Maimoun *et al.*[75]). Similarly, Minaire *et al.*[80] report a plateau BMD level after 25 weeks of SCI. In an effort to accommodate the SCI observations, we combined observations of NHANES III[99] and Cummings *et al.*[24] to estimate that the maximum percentage loss in an astronaut's BMD can be represented by a Gaussian distribution of 60 ± 17% (maximum 69%) relative to the astronaut's pre-flight BMD.

We compared our model against several terrestrial studies on lumbar spine fracture which contained a variety of measures of bone density. In order to make quantitative comparisons to those studies, we developed corresponding relationships for age-dependent bone mineral density for men and women that reflect the general population. For women, we used the research on pre- and post-menopausal women by Greer *et al.*,[50] which captured the significant decrease in BMD that occurs in women starting at about age 40 through a correction accounting for time elapsed since menopause. For men, we derived BMD from Mussolino *et al.*[89] through a linear decrease of BMD with age. We used the data of Ebbesen *et al.*,[31] which presented both BMD and bone mineral content (BMC), to convert our fracture model from dependence on BMD to BMC when necessary. Some studies used volumetric bone mineral density (vBMD), which normalizes the BMD with the volume, which can be represented in the ideal case as a cylinder with specified cross-sectional area and length.

Fracture Models

Many studies have sought to correlate bone strength with the loading conditions leading to fracture. There are varied approaches predicated on a critical skeletal

loading,[10,11,13,18,29,31,34,70,86,90,96,97,117,120] or, alternatively, a critical skeletal stress.[29,31,34,90,96,97] Independent variables include some measure of bone density, and, in some cases, bone geometry,[11,13,23,34,47,131] structure,[33,36,46,52,81,82,95,103,119] and load orientation,[14,23,29,43,52,60,101,122,128] among others. Ebbesen *et al.*[31] quantitatively assessed some of these correlations by characterizing bone density (bone mineral density (BMD), bone mineral content (BMC), and ash density), geometry (vertebral cross-sectional area) and failure conditions for L3 vertebrae under uniaxial compression (sample size $n = 101$). In one of their findings, they concluded that BMD is better correlated to the applied load at fracture than to the applied stress. Since we have access to BMD data that represent flight-ready astronauts, we used BMD and fracture load (FL) as the quantities of measure in our fracture models.

A sampling of cadaveric studies clearly points to a general trend of increasing bone strength with increasing BMD at the lumbar spine[31,86,90,117] and the proximal femur,[8,18,51,63] particularly within a specific age group.[55] Cheng *et al.*[18] was the primary source of data relating proximal femur BMD to FL for this analysis. As is typical in such studies, the age range of the cadavers (69 ± 15 years of age) was substantially above the average age of the mission-ready astronaut corps (45 ± 5 years of age[91]). A linear curve fit of the gender-specific data is shown in Fig. 2a. Women tend to have a slightly lower fracture tolerance at a particular BMD, which may be due to their typically smaller femoral neck cross-sectional areas and the differences in the bone microstructure due to aging.[57]

Changing the orientation of the loading can cause complicated stress states in which the bone fails as a result of tensile, compressive or torsional stresses, bending moments, or some combination of all these modes. Keyak *et al.*[60] found that an impact onto the posterolateral aspect of the greater trochanter produced the smallest fracture load. Ford *et al.*[43] observed that femoral structural capacity decreased by 26% when the loading direction relative to the femoral neck axis changed from 0° (purely lateral impact) to 45° (posterolateral impact). Pinilla *et al.*[101] found that variation in the loading angle from 0° to 30° (corresponding to the hip rolled slightly forward to backward, respectively) produced a 24% decrease in FL, which was as significant as the reduction in FL due to 25 years of age-related bone loss after the age of 65. We used this data to include uncertainty in the angle of impact in the femoral fracture model.

Several *ex vivo* cadaver studies, identified in Table 2, were used as a basis for the relationship between FL and BMD for vertebral fracture.[31,70,90,117] In contrast to the experimental data on the trochanter, studies have not yet found gender-dependent associations of FL with vertebral BMD in a statistically significant way.[31,33] In all datasets used in our model, vertebrae were exposed to steadily increasing uniaxial compression until fracture occurred. Ebbesen *et al.*[31] concluded that a linear fit was adequate to describe the FL/BMD relationship in their BMD range, although they found that a quadratic fit was slightly superior. We therefore used simple linear segments for the FL dependence on BMD (Fig. 2b). To ensure that the FL remained nonzero for all BMD, we used a severely osteoporitic population[70] for BMD < 0.4 (red line in Fig. 2b). For static loading at BMD ≥ 0.4, we pooled two of the studies[31,117] with similar demographics and experimental conditions to broaden the dataset and introduce the effect of spinal location (blue line in Fig. 2b). Biggeman *et al.*[10] estimated that the FL at the L3

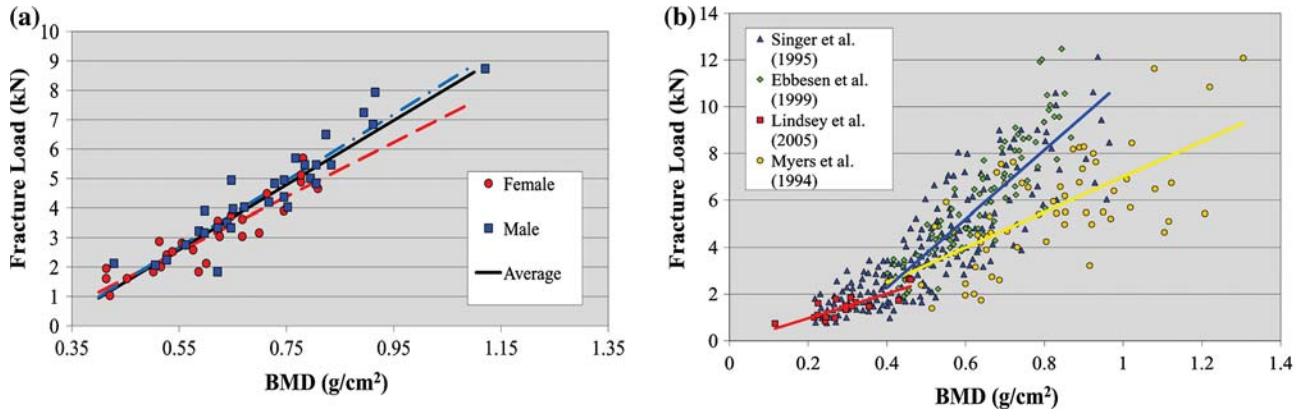

FIGURE 2. Fracture load (FL) as a function of bone mass used in BFxRM with underlying datasets. (a) Hip fracture model: Dependence of FL on trochanter BMD during a fall to the side. Linear fits for men (M) and women (F) were developed from Cheng *et al.*[18] (b) Lumbar spine (LS) fracture model: For BMD < 0.4, the fracture model follows the data of Lindsey *et al.*[70] For higher BMD, static loads are represented by the combined data of Ebbesen *et al.*[31] and Singer *et al.*,[117] while dynamic loads follow the data of Myers and Wilson.[90]

TABLE 2. Attributes of key bone fracture studies in which vertebral specimens were subjected to uniaxial compressive loading.

Population	Age (years) Mean ± SD, range	*n*	Vertebral level	Loading rate (mm/s)	BMD (g/cm^2) Mean ± SD	FL/BMD slope (kN/g/cm^2)	References
8F, 10M	66 ± 17.3, 29–89	287	T1–L5	0.004	0.515 ± 0.178	11.6	Singer *et al.*[117]
51F, 50M	57.1, 18–96	101	L3	0.083	0.617 ± 0.133	17.3	Ebbesen *et al.*[31]
13F	72.5 ± 9.7	18	T7–T11	0.423	0.294 ± 0.672	5.3	Lindsey *et al.*[70]
6F, 16M	52–75	61	L3–L5	1.500	0.809 ± 0.201	7.5	Myers and Wilson[90]

vertebral level changed by approximately ±0.3 kN per spinal segment during uniaxial compression. In the BFxRM, we do not attempt to determine the vertebral level at which fracture occurs, which would require a more sophisticated model incorporating detailed bone geometry, density, and microstructure, along with their complex interplay with applied loads through computation of localized stresses and strains. While computationally intensive studies of skeletal components subjected to well-defined loads are available,[22,23,25,52,60,81,103,133] it is impractical to implement this type of model within a widely ranging probabilistic model. Singer *et al.*'s[117] comparison of seven studies detailing fracture as a function of spinal location qualitatively supports the assertion that age is a more important factor than spinal location in determining FL (see their Fig. 6). Insufficient data is available in the literature to quantitatively establish the effect of loading rate on fracture, but when BMD is in the moderate to high range, it may suggest that the slope of FL vs. BMD curve decreases with increasing loading rate. (See Table 2; this trend continues in,[96,97] albeit with relatively sparse data.) The dominant failure mode under static loading is that of a crush fracture. However, more complex failure modes, such as burst fracture, can also occur with dynamic loading.[9,133] We are unable to capture such high-energy phenomena with the available data, but we did base our dynamic loading calculations on a dataset at a higher loading rate[90] for BMD ≥ 0.4 (yellow line in Fig. 2b).

The BMD of the wrist does not significantly change over the course of a space mission.[68] Therefore, wrist BMD was assumed to remain constant over time, and wrist FL was not modeled as a function of BMD. Rather, the wrist FL was specified with a Gaussian distribution based on strength measurements of cadaver specimens.[54] Wu *et al.*[135] performed cadaveric testing to determine the FL of the wrist, but their specimens were from an elderly population, and direct use of those results in our model would have underestimated the wrist strength of our population of interest. Instead, we obtained wrist BMD data from a cohort of healthy subjects between the ages of 20 and 59 years (0.515 ± 0.064 g/cm^2 for males, 0.434 ± 0.06 g/cm^2 for females).[1,79] We then applied this distribution to the relationship between wrist BMD and FL established by Wu *et al.*[135] to obtain wrist strength distributions used in our model for men (3439 ± 782 N, range 1875–5003 N) and women (2560 ± 629 N, range 1302–3818 N).

Biomechanical Loading Models

We developed four biomechanical loading models to estimate the loading at the most vulnerable skeletal locations during specific events. The events represent both routine tasks, such as a load to the spine while lifting a heavy object, as well as accidental falls or intentional jumps. The loading models include:

1. the load on the lumbar spine (LS) while holding a load with the trunk flexed (LS static lift, Fig. 3a);
2. the load on the femoral neck (FN) resulting from a fall to the side (FN side fall, Fig. 3b);
3. the load on the LS at impact after a fall from a height but landing on two feet (LS feet-first fall, Fig. 3c); and
4. the load on the outstretched wrist (W) in response to a side fall or other impact in which sufficient time exists for the astronaut to actively respond (W side fall, Fig. 3d).

In keeping with the philosophy of simplicity, the interactions are modeled as the sum of moments about the waist for the static lift, or as linear springs, dampers and masses for all the others. The LS static lift model (Fig. 3a), represents the slow lift or holding of a heavy object through a linked-segment model of the body in a flexed trunk posture. The sum of the forces and moments about the waist were used to compute the vertebral compressive force.[11,15,19,29,112] The overall erect body height, h_{tot}, is modeled as a linear function of body weight with slope and a distribution of intercepts defined in Table 3. The slope, $dh_{tot}/dm_{tot}g_e$, is fixed and the intercept, h_{tot_offset}, is parameterized to provide the population variation, so that a random choice of body mass leads to a corresponding distribution of h_{tot}. Similarly, the height of the upper body, h_{UB}, is modeled as a linear function of h_{tot} with a characteristic slope and intercept

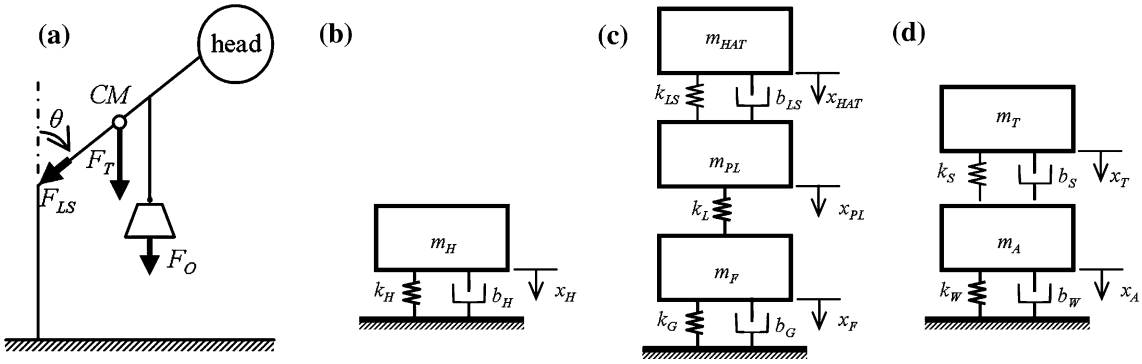

FIGURE 3. Biomechanical models. (a) Static lift model. A heavy object with a load F_O is held or slowly lifted at flexion angle θ. Combined with the load imposed by the torso F_T applied at the torso's center of mass (CoM), there is a resultant force on the lumbar spine F_{LS}, creating a net zero moment about the waist. Moment arms l_{WaS}, l_{CoM} and l_{PS} are documented in Table 3. (b) Femoral neck (FN) loading due to a fall to the side. The effective mass of the hip (m_H), the stiffness (k_H) and damping coefficients (b_H) of the hip pad, and the displacement of the hip x_H are shown. (c) Lumbar spine (LS) loading in a feet-first landing. The mass of the head, arms and trunk (m_{HAT}), pelvis and legs (m_{PL}), and feet (m_F); the stiffness of lumbar spine (k_{LS}), legs (k_L), and ground (k_G); the damping characteristics of lumbar spine (b_{LS}), and ground (b_G); and the displacement of the head, arms and torso (x_{HAT}), the pelvis and legs (x_{PL}), and feet (x_F) are shown. (d) Wrist impact model. The mass of the torso (m_T) and arms (m_A), the stiffness of the shoulder (k_S) and wrist (k_W), the damping characteristics of the shoulder (b_S) and wrist (b_W), and the displacement of the torso (x_T) and the arms (x_A) are shown.

distribution (Table 3). The distance between the waist and the shoulder, l_{WaS}, is represented as a percentage of h_{UB} by multiplying a coefficient, a, with h_{UB} and added to an offset. The distance between the waist and the torso's center of mass (CM), denoted l_{CM}, is specified in the same fashion. This method enforced dependency among the characteristic body dimensions, ensuring that no unrealistic combination of parameters would be used in the calculations. Assuming static equilibrium, the forces and moments at the lumbar spine due to the weight of the upper body, F_T, and the load held, F_O, are balanced by the postural muscle force, F_{PM}. We used anthropometric data to characterize the distance between the waist and the postural muscles, l_{PM}. (See Table 3 for all relevant values and the studies from which they were derived.) In addition to the variation in astronaut parameters that were included in the Monte Carlo simulations, we also included a triangular distribution for the weight of the lifted object in the range of 0 to 60 kg, with 20 kg being the most likely value based on mission design requirements.[37,38]

Figures 3b–3d display mass m, stiffness coefficient k, damping coefficient b, and displacement x for the hip (H), lumbar spine (LS), legs (L), feet (F), arms (A), ground (G), torso (T) and wrist (W). These variables form a system of first-order differential equations in time, t, with unknowns x and velocity $\dot{x}$ of the form:

$$m\ddot{x} + b\dot{x} + kx = mg$$

where g is the gravitational acceleration. The initial conditions are zero displacement, $x_0 = 0$, and initial impact velocity, $\dot{x}_0 = \sqrt{2gh}$, where h is the height of the fall. We did not consider the effect of atmospheric drag on a subject falling from a standing position or a vertical drop of 2 m or less due to the low maximum velocity achieved over such a short distance. This assumption is even better on the moon, which has no measurable atmosphere, and on Mars with approximately 1% of earth's density at its surface.[35] The values used for all parameters in the calculations and the datasets from which they were derived are shown in Table 3. Where more than one reference is cited, we used a simple bootstrap method to combine the data into values for our model. The total body mass, m_{tot}, varied by gender. If the scenario called for an astronaut to be outside the spacecraft on an extra-vehicular activity, we added 82 kg[124] to account for the additional mass of the spacesuit. We modeled all distributions as Gaussian, unless otherwise noted. For the falls to the side, the fall height h_H was the distance between the hip and the ground, modeled as a linear function of body mass m_{tot}, which is presented in Table 3 as a slope and offset. We held the slope fixed and defined a distribution of offsets to account for population variation. The torso is modeled as a percentage of total body mass using a uniform distribution between 0.3 and 0.5, less the mass of the arm. For feet-first drop landings, the fall heights used in the calculation of impact velocity were 1, 2, and 6.67 m for the astronaut predictions. For the validation studies, we used a normal distribution corresponding to the comparison data. The full matrix equations used for the dynamic models are given in Appendix B.

The loading model for the hip during a fall to the side was based on Robinovitch *et al.*[109] As shown in Fig. 3b, the model used a single mass representing the effective mass of the hip (H), one spring representing

TABLE 3. Parameters used in the four biomechanical models shown in Fig. 3.

Parameter	Units	Value ± SD Min/max	Source
m_{tot}	kg	60.73 ± 8.25 (F) 85.15 ± 0.13 (M) 50/114	NASA Publications,[2,76] Naval Biodynamics Laboratory[3]
Static lift model			
$dh_{tot}/dm_{tot}\,g_e$	cm/N	0.072	NASA Publications,[2,76] Naval Biodynamics Laboratory[3]
h_{tot_offset}	cm	120.62 ± 2.2 116/125.2	NASA Publications,[2,76] Naval Biodynamics Laboratory[3]
dh_{UB}/dh_{tot}	cm/cm	0.38	NASA Publications,[2,76] Naval Biodynamics Laboratory[3]
h_{UB_offset}	cm	1.73 ± 5.77 −10.72/14.19	NASA Publications,[2,76] Naval Biodynamics Laboratory[3]
dl_{WaS}/dh_{UB}	cm/cm	0.77	NASA Publications,[2,76] Naval Biodynamics Laboratory[3]
l_{WaS_offset}	cm	−9.98 ± 7.53 −25.75/5.78	NASA Publications,[2,76] Naval Biodynamics Laboratory[3]
dl_{CM}/dh_{UB}	cm/cm	0.44	NASA Publications,[2,76] Naval Biodynamics Laboratory[3]
l_{CM_offset}	cm	9.95 ± 10.99 −13.78/33.69	NASA Publications,[2,76] Naval Biodynamics Laboratory[3]
l_{PM}	cm	5.26 ± 0.3 4.77/5.76 (M) 4.83 ± 0.45 4.1/5.6 (F)	Chaffin and Baker,[16] Marras and Sommerich,[77] Moga *et al.*[84]
Hip impact model			
a_a	None	0.12 ± 0.37 0/1	Sabick *et al.*[110]
a_H	None	0.5 ± 0.081	Robinovitch *et al.*[109]
a_s	None	0.27 ± 0.17	Kannus *et al.*[58]
k_H	kN/m	49.6 ± 19.8 (F) 57.7 ± 7.0 (M)	Robinovitch *et al.*[109]
b_H	kN s/m	0.754 ± 0.207	Robinovitch *et al.*[109]
dh_H/dm_{tot}	m/kg	0.0053	NASA Publications,[2,76] Naval Biodynamics Laboratory[3]
h_{H_offset}	m	0.514 ± 0.019 0.473/0.554	NASA Publications,[2,76] Naval Biodynamics Laboratory[3]
k_{LS}	kN/m	3360E ± 3300 190/7800	Prasad and King,[104] Renau *et al.*,[105] Duma *et al.*,[30] Yoganandan *et al.*[137]
k_L	kN/m	34.3 ± 11.0 1145/5850	Fiolkowski *et al.*,[42] Chi and Schmitt,[19] Lafortune *et al.*,[64] Arampatzis *et al.*,[4–7] Granata *et al.*,[49] Ferris *et al.*,[40,41] Padua *et al.*[100]
k_G	kN/m	177 ± 157 76.0/411	Chi and Schmitt,[19] Arampatzis *et al.*,[4,7] Moritz and Farley[85]
b_{LS}	kN s/m	1290 ± 642 1290 − 2*SD/1290 + 2*SD	Prasad and King,[104] Izambert *et al.*[56]
b_G	kN s/m	1500 ± 10% 1500 − 0.2*b_G/1500 + 0.2*b_G	Chi and Schmitt[19]
Wrist impact model			
a_A	none	0.0474	NASA Publications,[2,76] Naval Biodynamics Laboratory[3]
m_{A_offset}	kg	0.17 ± 0.084	NASA Publications,[2,76] Naval Biodynamics Laboratory[3]
a_T	none	0.3/0.5	NASA Publications,[2,76] Naval Biodynamics Laboratory[3]
k_S	kN/m	2.4163 ± 1.137	Chiu and Robinovitch,[20] Davidson *et al.*[26]
k_W	kN/m	48.0 ± 100 (minimum set to 10)	MacNeil and Boyd,[74] Muller *et al.*,[88] Chiu and Robinovitch,[20] Davidson *et al.*,[26] Staebler *et al.*,[121] Pistoia *et al.*[102]
b_S	kN s/m	0.24142 ± 0.0889	Chiu and Robinovitch[20] and Davidson *et al.*[26]
b_W	kN s/m	0.42204 ± 0.30706	Davidson *et al.*[26]

Gender-specific values are denoted as (F) and (M).

the stiffness of the hip pad, and one damper representing the damping characteristics of the hip pad.[109] The effective mass of the hip was defined in the Robinovitch[109] model as the mass of the body from under the arms to the knees. A comparable percentage of overall body weight, a_H, was used as a multiplier to the total body weight within the model to determine the effective mass m_{eff}. The percentage was determined from sources with astronaut anthropometric data[2,3,76] and could range from upper:lower ratios of 40%:60% to 60%:40%. Our calculation of the force transmitted to the proximal femur during standing falls on earth

and in the reduced gravity environments of the moon and Mars were augmented to account for:

1. the direction of fall.[14,43,101,128] In the calculation, the hip impact angle β was randomly distributed from 0 to $\pi/6$ (0–30°) for any given event. The impact force (see Appendix B) was then attenuated by the multiplier $(1 - \beta)$[14,43];
2. the active response to the fall. This response was set to be successful 72% of the time[53] and, if successful, further reduced the load by a multiplier $(1 - a_a)$, where the attenuation due to active response, $a_a = 0.12 \pm 0.37$, is between 0 and 1[110];
3. estimates regarding the contribution of the EVA suit to fall impact dynamics, primarily by increasing both the body mass and hip padding. Based on hip protector attenuation data,[58] our model suit attenuation, a_s, reduced the force at impact by a multiplier of 0.27 ± 0.17.

The LS feet-first fall was based on a mass/spring/damper model, similar to those developed by others.[19,20,26,83] As shown in Fig. 3c, it incorporated three lumped masses (head, arms and trunk (HAT); pelvis and legs (PL); and feet (F)), a spring and damper between the HAT mass and the PL mass to represent the stiffness and damping characteristics of the lumbar spine,[30,56,104,105] a spring between the PL mass and the F mass to represent the stiffness characteristics of the legs,[4–7,19,39,40,42,49,64,100] and a spring and damper between the F mass and ground to represent the stiffness and damping characteristics at the ground.[4,7,19,40,41,85]

The loading model for the wrist when it is used to break a fall was based on Chiu and Robinovitch.[20] As shown in Fig. 3d, the model incorporated two masses (torso (T), and arm (A)), a spring and damper between the masses to represent the stiffness and damping characteristics of the shoulder (S),[20,26] and a spring and damper between the arm mass and ground to represent the stiffness and damping characteristics of the wrist (W).[26,74,87,102,121] See Table 3 for further details.

The Fracture Risk Index and the Probability of Fracture

The simulation framework estimates fracture risk through computing the fracture risk index (FRI), sometimes called the factor of risk, which compares the load imposed on the bone and the maximum skeletal load that can be applied before fracture occurs.[51] Although there are a range of definitions for FRI (or FOR) in the literature, we used the most direct form, defined as the ratio of the applied load (AL) to the fracture load (FL).[51] In this form, the FRI creates a deceptively simple framework upon which to develop bone fracture risk estimates. By design, if FRI < 1, there is a lower risk of fracture; conversely, if FRI > 1, there is a higher likelihood of fracture.[51] The challenge in using this form of FRI is in providing skeletal loading estimates and local skeletal strength estimates that are faithful analogs to the scenario being modeled. Based on the "keep it simple" philosophy of this analysis and the type of data available for the modeling effort, FRI was used as the principal fracture risk forecast metric.

Although this approach yields a great deal of qualitative insight, more useful forecasting requires a more quantitative measure indicating the fracture probability. Review of the current literature reveals few studies that have attempted to link FRI directly to the probability of fracture, aside from stated assumptions that FRI ~ 1 or greater indicates a likely fracture. To do better, we computed the probability of fracture from the FRI estimates, following the approach of Davidson *et al.*[26] Additionally, the FRI calculations are combined with knowledge of the incidence rates to predict a probability over a defined period of time. Details of this transformation are given in Appendix A.

Scenario Execution

For each of the four mission scenarios (see Table 1), four biomechanical models and both genders, we carried out a Monte Carlo probabilistic simulation to predict the risk of fracture for one crew member during the course of the mission. The chief simulation tool was the commercially available Crystal Ball (Oracle, Inc.) environment, which operates on top of Microsoft Excel. The code permitted easy definition of parameter distributions, as well as the execution of many thousands of trials that sample these parameters to generate the range of possible outcomes. Each simulation used either Monte Carlo sampling or Latin hypercube sampling techniques, based on the most appropriate technique for the data set. The latter is preferable in most cases due to its more complete coverage of the distribution function outliers.

Figure 4 outlines an example of the runtime procedure for the FN side fall model (Fig. 3b); refer to Table 3 for all parameters and distributions. Figure 4a provides an overview of the process, while Figs. 4b and 4c detail the steps formed within the biomechanical and fracture models, respectively. Top-level input data included: whether the event occurred during an extravehicular activity or an intra-vehicular activity; the gravitational level, g; astronaut gender; and the mission timeline.

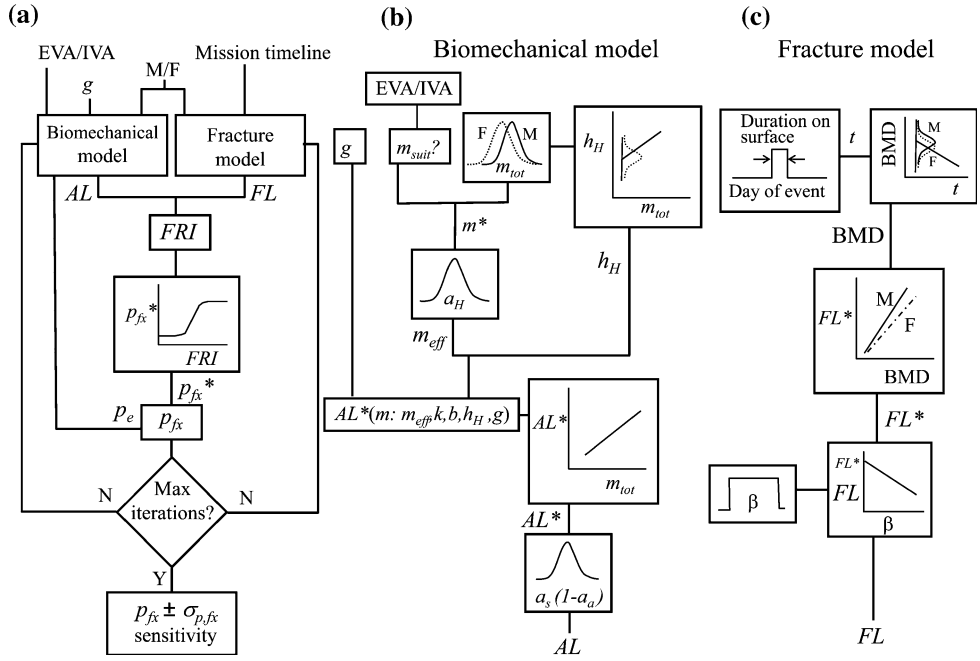

FIGURE 4. Outline of scenario execution for the femoral neck side impact model. (a) Top-level schematic for the Monte Carlo simulation. (b) Biomechanical model, responsible for producing the applied load. (c) Fracture model, responsible for producing the fracture load.

Prior to the Monte Carlo simulations, we solved a system of ordinary differential equations resulting from the mass/spring/damper model (Appendix B), using Mathworks, Inc.'s MATLAB to form a relationship between an interim value of the applied load at the skeletal location of interest, AL*, and the total body mass, m_{tot}. The procedure, shown in Fig. 4b, is: Specify gender and whether or not the scenario called for an EVA. Using the gender-specific distribution for m_{tot}, we separated the permissible range on m_{tot} into eight intervals. We added the mass of the spacesuit to the total body mass, m_{tot}, if an EVA was being examined to compute the total mass at impact, m^*. This mass was reduced by a multiplier, a_{H}, to determine an effective mass, m_{eff}, representing the portion of m^* that actually contributed to the forces at impact. Meanwhile, m_{tot} was also used to determine a characteristic height at the hip level, h_{H}, defined through a linear relationship to m_{tot}. The slope, $dh_{\text{H}}/dm_{\text{tot}}$, was fixed, and the intercept $h_{\text{H\_offset}}$, provided the population variability. The fall height in this case corresponds to h_{H}, which was used in the calculation of the impact force and velocity. For each interval, we solved the set of ODEs (Appendix B) using values for the mass, height, spring and damper coefficients that reflected the relevant distribution of each parameter. The resulting solution included the unknown displacement, x, and velocity, $\dot{x}$. Next, we calculated the ground reaction force $F_{\text{GR}} = b\dot{x} + kx$ from the solution, which is equivalent to AL* for this biomechanical model. We saved the resulting AL* for convergence analysis, along with the mean m_{tot} of the interval. We then repeated the process with new values for m_{tot}, k, and b. We tested the effect of running 5000, 10,000 and 50,000 parametric iterations and concluded that negligible changes in the mean AL* occurred beyond 5000 iterations. The results of the calculation were 8 pairs of m_{tot} and AL*, which could then be curve fit. For the hip impact model, a linear fit of AL*(m_{tot}) sufficed to define the relationship, although a quadratic fit was necessary for the more complicated lumbar spine drop model. Finally, we built the function AL*(m_{tot}) for each gender, EVA/IVA, and g into the Monte Carlo engine.

For every trial of the Monte Carlo simulation, the biomechanical model (Fig. 4b) sampled m_{tot}, as specified by the distribution in Table 3, and calculated the corresponding AL*(m_{tot}) for the gender, EVA/IVA, and g under consideration. As described above, the function implicitly includes the population variability in k, b, and h_{H}. The interim load was multiplied by: (1) the suit attenuation factor, a_{S}; and (2) the active response attenuation factor $(1 - a_{\text{a}})$. The factor a_{a} assumed a non-zero value 72% of the time, representing the likelihood of a successful active response. The result was the output of the biomechanical model, i.e., the AL to the proximal femur.

In the fracture model (Fig. 4c), inputs include gender and mission timeline. Each trial of the Monte Carlo simulation selected a mission day based on a uniform distribution function during the time that the astronauts were on the surface of the moon or Mars. The

gender specified a pre-flight BMD distribution function representing the astronaut population from which the Monte Carlo trial chose a pre-flight BMD. Then, these selections were used to evaluate BMD on the day of the fall through the empirical time-dependent bone loss relation. The computed change in BMD was compared against a second estimate of the change in BMD, which was based on the loss plateau observed in terrestrial studies of spinal cord injury. The two values were tested, and the minimum BMD loss was chosen. The resulting BMD was used to find an interim fracture load, FL*. In the last stage, a postero-lateral impact angle β between 0 and $\pi/6$ was randomly selected. The fracture load, FL, was evaluated as FL$(1 - \beta)$ and returned as the output of the fracture model.

Referring back to Fig. 4a, the ratio FL/AL was formed to find the fracture risk index, FRI. Using the procedure outlined in Appendix A, FRI was converted to an interim fracture probability p^*_{fx}. The probability that a fall event would occur on a given day, p_{e}, was built into the model based on Apollo data. Next, p^*_{fx} was multiplied by p_{e} to form the probability of fracture, p_{fx}.

This procedure represents a single trial in a Monte Carlo simulation of femoral fracture. Typically, each simulation required between 50,000 and 100,000 trials. When the variation of the standard deviation of the output parameters remained less than 0.01 over 2500 trials, we considered the solution to be converged. The primary data resulting from each simulation were a mean and standard deviation for p_{fx}, sensitivity analysis (internally calculated by Crystal Ball), and the probability density function of FRI. The other simulations for astronaut prediction and validation departed somewhat from this procedure on specifics, although the general construction remained the same. For example, the lumbar spine fracture model did not include gender dependence or the effect of off-axis impact, but it did include a relevant modification for impacts of short vs. long duration. In the validation simulations, the distributions were varied to correspond to the population under investigation.

RESULTS

Biggeman *et al.*[10] estimated the fracture load (FL) of the L3 vertebra for 75 patients (53F, 22M, 15–88 years of age) based on measurements of the trabecular bone density and the endplate area. The study included pre-fracture volumetric bone mineral density (vBMD) from live subjects and compressive testing on cadavers. In this study, none of the patients were known to have cancer, osteolytic or osteoblastic destruction. In a similar study, Bouxsein *et al.*[11] also calculated the FL as a function of age for 375 women

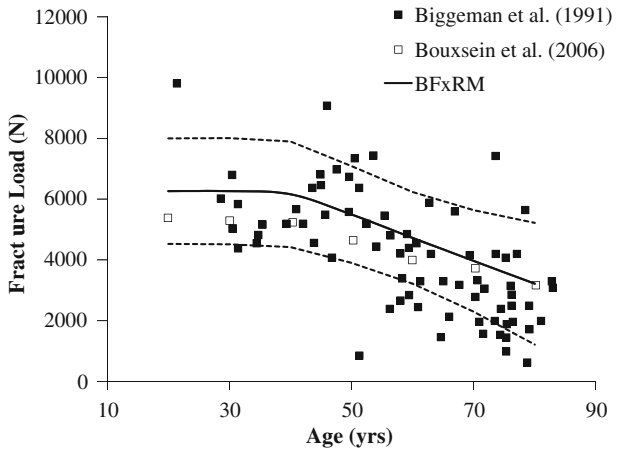

FIGURE 5. Comparison of BFxRM predictions of fracture load as a function of age with data from Bouxsein *et al.*[11] and Biggeman *et al.*[10] Solid line represents BFxRM simulation mean value, while the dotted lines denote the uncertainty band of ±3SD.

between 21 and 97 years old to assess the risk of fracture while lifting a 10 kg load with a trunk flexion of 90°. The FL was calculated from vBMD, the cross-sectional area of the vertebral body, the elastic modulus of bone and a correlation factor. When compared with the predictions of our model in Fig. 5, 100% of the Bouxsein data and 75% of the Biggeman data is bounded within our uncertainty band (dotted lines in Fig. 5). Due to the relatively large number of women in the sample, our prediction shows a definitive decline in bone strength after age 40. (Our age vs. BMD relationship accounted for the large decline in BMD due to the loss of bone mass that occurs after menopause.[50]) The BFxRM functions well, even when the age of the population varies more widely than that of the astronaut corps (45 ± 5 years).

BFxRM calculations of the applied load for the wrist and LS impact models and the static lift model performed extremely well against experimental measurements and calculations of forces (Fig. 6). Most of the experimental data is from healthy young male and female competitive athletes, recreational athletes and students, ranging in age from 18 to 35 years. Although the astronaut corps tends to be older than these cohorts, they are highly fit, so we consider these studies to be a good representation of our target population. In addition, data from children (7.4 ± 2.2 years), adolescents (16.1 ± 1.3 years), cadavers (64–86 years) and mechanical surrogates were also used to show that the model accounts for the uncertainty associated with differences between populations. For the wrist impact model, we tested BFxRM results against seven sets of experimental measurements of the ground reaction force, F_{GR} (Fig. 6a).[20,21,26,27,61,71,73] (See Appendix B for the details of the F_{GR} calculation.) In the case of

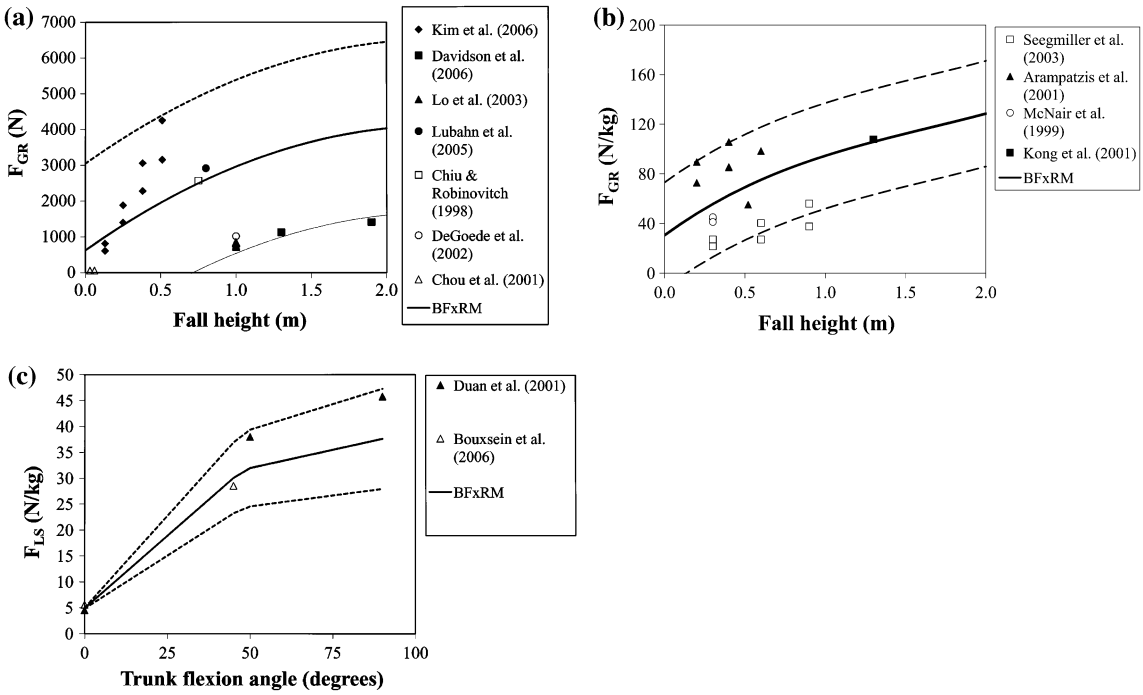

FIGURE 6. Comparison of BFxRM prediction of forces with experimental data for: (a) the wrist impact model F_{GR}[20,21,26,27,61,71,73]; (b) the lumbar spine static lift ground reaction force (F_{GR})[4,6,7,62,78,113]; and (c) the static lift lumbar spine force (F_{LS}) as a function of trunk flexion angle.[11,29] Solid line is BFxRM mean predicted value, while dotted lines represent the uncertainty band.

the lumbar spine static lift model, we compared the BFxRM predictions of F_{GR} to four experimental studies in which F_{GR} was measured during a drop landing (Fig. 6b).[4,6,7,62] We compared the predictions of Duan *et al.*[29] and Bouxsein *et al.*[11] with BFxRM predictions with regard to the effect of trunk flexion angle on the force generated at the lumbar spine while holding a 10 kg load (Fig. 6c). The minimum force is generated in an upright posture, while the maximum can be approximately 10 times greater with a flexion angle of 90°. The BFxRM model performed equally well when compared to the case of no load (data not shown).

The next set of simulations compared the predicted fracture risk index to that of other studies. The proximal femur is one of the most studied osteoporotic fracture locations, and it is one of the most prominent locations exhibiting microgravity bone loss in astronauts. Lang and co-workers[59,65] performed finite element simulations of bone fracture using BMD data from 11 astronauts. Their calculation of risk factor was 2.1 ± 0.47 for the 11 astronauts in the study when a simulated posterolateral fall was used as the loading event. To validate our FN side fall model, we configured the BFxRM inputs to match a pre-flight fracture prediction and compared our results against the well accepted, higher fidelity model (Fig. 7). The uncertainty in our model is approximately double that of the

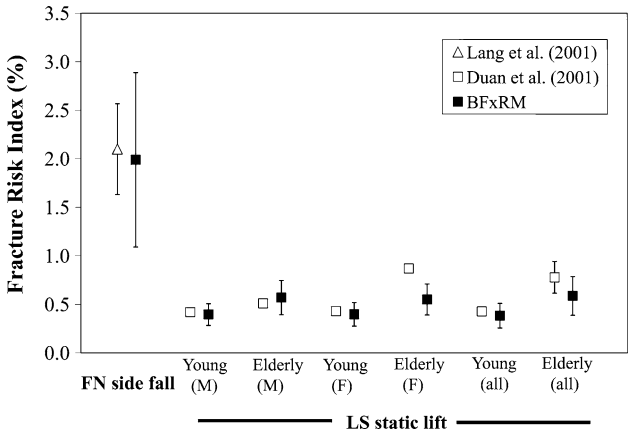

FIGURE 7. Comparison of calculated FRI to BFxRM predictions for pre-flight unhindered posteriolateral fall[65]; and static lift of 10 kg load.[29]

Lang study. This is not surprising since we employed general population measures in our model rather than the specific range of BMD levels of the 11 astronauts used in the Lang study.

The other data comparisons shown in Fig. 7 are based on a study of spinal loads during a static lift. Duan *et al.*[29] grouped subjects into two age ranges: young (18–43 years) and elderly (60–92 years). The mean and standard deviation of their FRI falls within our uncertainty band, except for the case of elderly

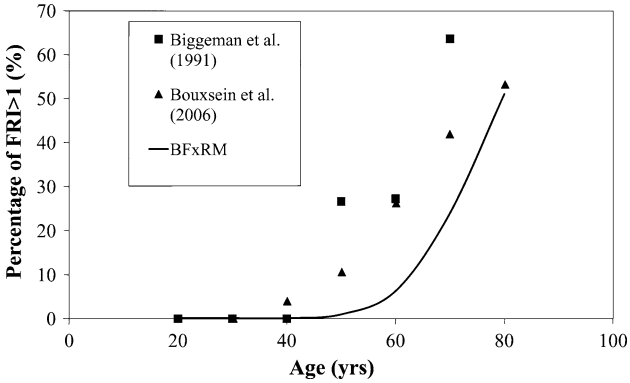

FIGURE 8. Comparison of the BFxRM FRI calculation with the calculations of Bouxsein *et al.*[11] and Biggeman *et al.*[10] on the percentage of FRI > 1 in a static lift.

females in which the BFxRM calculations are conservative compared to Duan *et al.*'s predictions.

Model sensitivity analysis illustrates the relative change in the output parameters due to small changes in each input parameter, assuming all other inputs are held constant. Such sensitivity analyses provide a clear understanding of which parameters most affect model outcome and contribute to the output uncertainty. It also identifies areas in which efforts can be focused in the future to reduce model uncertainty. The most sensitive parameters in the calculation of the proximal femur fracture probability are the parameters used to convert FRI to a probability, followed by the angle at which the load is applied and the attenuation afforded by the EVA suit. This is not an unexpected finding, in that these parameters have some of the highest uncertainty of all the input parameters within the model.

Bouxsein *et al.*[11] and Biggeman *et al.*[10] calculated the percentage of cases for which FRI > 1. In Fig. 8, our model shows the same trend as the predictions of these studies, although it predicts a lower absolute risk at the more advanced ages. Below BMD = 0.4 g/cm^2, our fracture model was created from a linear fit of a small dataset of elderly women. Although our results are arguably as valid as the comparison calculations, additional data in this BMD range would strengthen our confidence in the prediction of fracture risk for the elderly on earth.

The literature abounds with studies of spinal fracture incidence due to a fall from height, in which height is one of the many significant factors. The excellent study of Lapostalle *et al.*[66] indicated that the body configuration at impact was the most important factor in determining mortality, a finding that is reflected perhaps less explicitly in many other studies.[48,106,125,132] Since these studies by their nature are not well controlled in terms of the number of victims,

TABLE 4. Comparison of BFxRM predictions of spinal fracture in drop landings with population studies.

Reference	*h* Mean ± σ, min/max (m)	Spinal fracture incidence (%)	BFxRM prediction (%)
Lowenstein *et al.*[72]	6.9 ± 4.4, 2/21	50	56
Goonetileke[48]	3.2 ± 3.5, 0.8, 51.8	19	34

fall height, body configuration at impact, gender, surface properties, intentionality, or survival, it is challenging to find studies that adequately represent the scenario of interest.[93] In a feet-first landing following a fall from height, a range of studies indicate that the lower extremities and spine are frequently endangered.[47,98,111,118,130] We tested the BFxRM against two studies of the general population that specifically attempted to control for body configuration in a fall from height[48,72] (Table 4). Both of these small datasets were based on victims who did not ultimately survive the fall. Lowenstein *et al.*[72] considered strictly feet-first landing in their study of 12 casualties. Goonetileke[48] covered a broader range of body configurations in his comprehensive study (n = 146). His subset of 21 cases with upright landing includes both feet-first and knee-first impact. Also, the fall height in that study was given only in terms of the overall data, so the fall height we used in the calculations may not truly represent the correct parameters of the subsample. Finally, since we were not provided with an alternative, we used our standard body mass of 72.94 ± 6.94 kg in both cases. The BFxRM prediction performed well against the more relevant Lowenstein study, with a prediction that was within 6% of the reported incidence. The comparison is less persuasive for the Goonetileke study, although it should be expected to be less accurate due to reduced precision in fall height and the presence of another upright impact mode in the data.

Mission Predictions

In simulations of extra-vehicular activity (EVA) shown in Fig. 9, we assumed that the stiff 82-kg spacesuit would add to the mass of the astronaut, improve the padding to the hip, and limit the torso's bending angle to 45°. We suspect that the suit improves the fidelity of our idealized models through increasing the likelihood of a straight-arm impact in the wrist simulations and the likelihood of vertical two-footed landing in the lumbar spine dynamic calculations.

Femoral neck fracture probability due to a fall to the side during an EVA is very low even during a long-duration Mars mission, possibly due to the effective use of spacesuit padding (Fig. 9). The static lift model

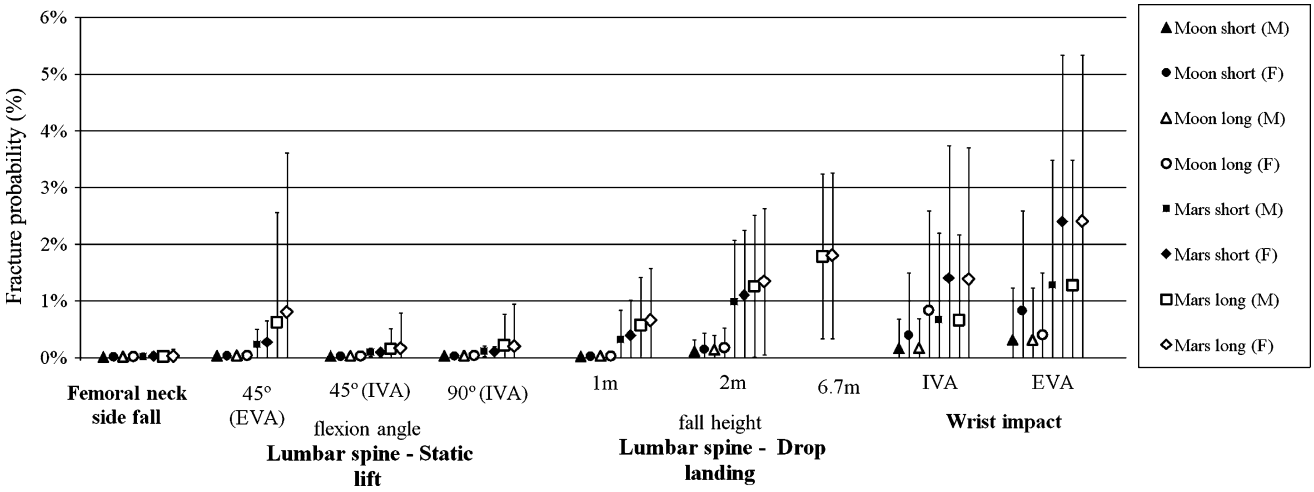

FIGURE 9. Predictions of bone fracture probability during reference missions to the moon and Mars. Open symbols denote the short missions as defined in Table 1, while closed symbols indicate the longer mission scenarios.

represents an astronaut slowly picking up or holding a heavy object (up to 60 kg, mean 20 kg) on Mars or the moon. The estimated probability of spinal fracture during an Intra-Vehicular Activity (IVA) in this scenario is similarly low, even at the most punishing flexion angle. However, the added weight and compromised bone integrity during an EVA on a Mars long-duration mission leads to a mean fracture probability of slightly less than 1%. Considering the disastrous consequences to the crew and the mission, this scenario warrants further consideration.

In the dynamic fall scenarios, we assumed that the crew was situated on the reduced-gravity surface of the moon or Mars. The probabilities are therefore based only on the portion of the mission that occurred on the surface. Based on workload requirements from lunar mission planning, we assumed that each astronaut had a similar workload and that any given crew member would perform 5 EVAs per week. Using Apollo data, we estimated that falls would occur approximately once per EVA and that a posterior lateral fall would transpire about once every 28 falls. We used these data to form incidence rates to calculate the probability that a posterior lateral fall event would occur on a given day, denoted as p_e. The ladder extending from the new Lunar Lander to the surface is currently designed as 20 ft. (6.67 m). We assumed that the Mars Lander would have a similar ladder. Documentation from the Apollo era indicates that it is not unusual for the astronauts to skip the rungs at the bottom of the ladder and instead jump down to the surface. We therefore examined drop heights of 1 or 2 m, as well as 6.67 m representing an accidental fall from the top of the ladder. The risk of spinal fracture due to a 1-m drop on short- and long-duration lunar missions is less than 0.1% at the 95th percentile. The corresponding probability for a lunar 2-m drop remains below 0.5%. The fracture probability on Mars is significantly higher due to extended time in space. The 95th percentile approaches 5%, and so this scenario merits further investigation. We found that the short and long missions to Mars had similar fracture risks, despite the briefer stay on the surface in the short mission scenario (see Table 1 and Fig. 9).

In a fall to the side, we assumed that the astronaut was initially standing on solid ground and impacted the ground with the hip. The natural response to such a fall is to extend a hand toward the ground to absorb some of the impact. While spacesuits are cumbersome and the field of view is limited, we assumed that only a proportion of the falls would be broken in this way. This kind of active response by the astronaut could protect the hip, but lead to a wrist fracture, which we found to be the most likely type of fracture (Fig. 9). While this type of injury is unlikely to be fatal, it can cause great discomfort and jeopardize mission success. The 95th percentile for Mars missions ranges from 5 to 8%, which is not insignificant. Gender-specific differences in mean wrist fracture probability are greater than that for fracture of the hip or lumbar spine. However, gender dependence does not approach statistical significance.

DISCUSSION

Current clinical practice with regard to bone health at NASA treats Dual energy X-ray Absorption (DXA) measurements as the gold standard. Most of the information related to astronaut bone health and bone loss is referenced to DXA measurements of bone mineral density (BMD). Essentially, DXA measurements

quantify the opacity of bone to X-ray energy. In the bone fracture risk model (BFxRM), we use BMD as the sole measure of bone strength. Clearly, this is simplistic.[69] It does not take into account the complexity of bone quality in terms of, e.g., its external bone geometry[11,13,23,34]; internal microarchitecture, structural properties, and remodeling[33,36,44–46,52,81,82,95,103,119,127]; failure mode[45,127]; or loading history.[45,70,123,126] Clinically, a lower BMD does not necessarily correspond to reduced bone strength due to the profound implications of these other factors on load propagation and bone failure.[69] However, we believe that the relation of FL to BMD is the most practical approach for probabilistic modeling of astronaut fracture risk at this time with the available data.

Instead of accounting for all parameters, we made every effort to find the studies that most closely matched astronaut demographics and skeletal loading situations to develop relationships between fracture load (FL) and BMD. However, experimental studies of FL, such as those used within this model, tend to have a preponderance of elderly subjects, as opposed to athletic, more youthful astronauts. Aging imposes a loss in the mineral content of bone, changes in bone geometry, and deterioration of the bone's microarchitecture that can all contribute to fracture susceptibility. At this time, we cannot answer the question of whether or not "space aging" of bone is comparable to that of aging bone on earth.

Our model pessimistically assumes that astronauts lose bone mass continuously during a mission at the rates observed with microgravity exposure, down to a minimum bone mass. Bedrest studies indicate that extensive resistive exercise can mitigate some disuse bone and muscle loss.[114] Based on reports of astronaut bone recovery upon return to earth,[116] several months may be necessary to recover 50% of the bone loss accumulated during extended missions (>130 days). Many biological processes depend intrinsically on reaching particular threshold values, so bone recovery may not be initiated on the moon or Mars when the astronaut is exposed to reduced gravity levels. Consequently, we could not justify including bone mass recovery or the inhibition of bone loss rate during a stay on Mars or the moon. These remain areas in which we are eager to incorporate new data into the BFxRM as it becomes available.

In spite of its simplicity, the BFxRM proves itself to be quite powerful in comparison of its predictions to a broad range of published experimental measurements and higher-fidelity computational models. Simple biomechanical models described hip fracture due to a fall to the side, spinal fracture in the cases of a static lift with trunk flexion and feet-first landing, and wrist fracture resulting from a fall. In testing these models, the prediction of FL as a function of age matched independent studies. The forces developed between the ground and the body and their transmission to specific regions of the skeleton were captured within the uncertainty band of our predictions. The prediction of the fracture risk index (FRI) captured all of the essential features in comparable models, both quantitatively and qualitatively. In these validation studies, our relationship between BMD and age for women included a correction for the time elapsed since menopause, which resulted in a slightly reduced fracture risk for the elderly as compared to the other studies.

The availability of studies in the literature permitted the inclusion of load orientation into the BFxRM model of femoral fracture. In a fall to the side, the failure load for the proximal femur is at a minimum for a posterolateral impact.[14,43,60] The failure can be governed by either tensile or compressive strains, depending on the loading direction and the bone geometry.[14] However, in the feet-first landing model, the BFxRM does not incorporate the effect of angular orientation on the propensity toward spinal fracture. Off-axis and/or torsional loading leads to an inhomogeneous stress distribution that is highly dependent on bone geometry, and the uniformity and anisotropy of its internal material properties. Bending and axial rigidity are related, but bending rigidity also depends on other factors such as vertebral depth.[23] For this reason, we attempted to restrict our comparison to literature on vertical feet-first landing onto hard surfaces. We did include a reduction in fracture resistance for dynamic loading (Fig. 2b). This simple model may not be sophisticated enough to capture the rich variety of impact configurations and force transmissions that occur in studies of terrestrial falls from height. Nevertheless, the model performed well, particularly in matching well-characterized samples from the general population.

Hip fracture was unlikely during extra-vehicular activity for any mission scenario (Fig. 9). Sensitivity analysis indicated that the spacesuit padding played a large role in hip protection, although the suit's bulk, lack of flexibility and peripheral vision are themselves culprits in the frequency of falls during EVAs. Modern, more form-fitting spacesuits may reduce fracture incidence by improving an astronaut's agility and field of view and by diminished mass. On the other hand, the increased range of motion could also place an astronaut at risk for spinal fracture during a momentary lapse in picking up a heavy object. It is unclear whether or not these attributes would affect the incidence of falls on the wrist. In any event, since wrist fracture was found to be the mostly likely type of bone fracture, the attenuation designed into the glove is an important consideration. Currently, our group is

conducting a study on the effect of padding on hip fracture. The BFxRM could also be used to aid in boot design and ladder configuration in order to minimize the risk of spinal fracture due to vertical drops. Finally, a multi-objective optimization meta-model (see, e.g., Branke *et al.*[12]) built on top of BFxRM could identify designs with reasonable trade-offs in the choice of materials and their mass and distribution through optimizing for comfort, functionality and fracture risk for either lunar or Martian missions.

No practical differences in fracture risk emerged in comparing our lunar short and long missions (see Table 1 and Fig. 9). Unsurprisingly, Mars missions carried significantly more risk than lunar missions due to increased bone loss. Fracture probability on Mars was relatively insensitive to increasing the duration of stay from 40 to 540 days, despite allowing fracture to occur only on the planet surface. No significant differences appeared when increasing outbound transit time somewhat from 162 to 189 days, although extending transit time should be expected to magnify fracture probability. Since fracture risk poses a threat to mission success, processing additional mission scenarios through this model (or in concert with a higher-level optimization algorithm) could aid in planning spacecraft trajectories, mission infrastructure, operations and risk mitigation strategies.

We have presented a strategy to predict fracture risk in unfamiliar environments. The purpose of this work is to winnow down the envelope of possibility in the broad strokes needed to plan space missions and identify areas that merit more scrutiny. A more precise prediction of fracture risk could be made in a detailed deterministic model when all relevant details regarding an individual and a loading event are available, including force transmission properties to a specific skeletal location, the spatial distribution of material properties within the bone, and a detailed representation of the bone geometry and surrounding tissue, as long as adequate computing power and time is available. A statistical approach as outlined here is a more fundamental step in approaching an unfamiliar set of circumstances. It can provide a tool to bound the problem for mission planning and to target scenarios that would most benefit from higher-fidelity numerical work and clinical studies. There are many sources of uncertainty in our model, and there is also room for sharpening our knowledge base and improving the fidelity of our predictions. We continue to search for additional relevant studies against which to compare the model. A key priority in future work is to verify the BFxRM model through comparison of fractures in a population that is clinically osteoporotic. We are working with clinical partners to gather statistical information in order to directly construct an FRI-to-probability relation as described in Appendix A using the current FRI calculation, thereby reducing the uncertainty in future estimates of fracture probability.

CONCLUSIONS

To produce a practical, useful estimate of astronaut fracture risk, we combined simple biomechanical loading models with simple, physics-based bone fracture models, based on carefully considered choices for the underlying data that ties the model equations to real life physics. We used the well-established Monte Carlo approach to characterize uncertainty. We derived model parameters from astronaut data for space mission scenarios whenever possible, and from populations that most closely matched that of the target cohort otherwise. When the nature of the loading and population was well-characterized, the model provided excellent performance in comparison to experimental data and calculations from higher fidelity models in terms of ground reaction forces, skeletal loading, fracture risk index (FRI), and probability of fracture. We seek further confirmation of our fracture model at low BMD, corresponding to the elderly on earth and astronauts after long periods in reduced gravity. At this time, it is unknown if the characteristics of bone microarchitecture of the latter is directly analogous to that of bone changes due to aging.

Predictions of hip, spinal and wrist fracture probability during reference lunar and Martian missions indicated that the risk of hip fracture is low in all missions, despite the potential for substantial loss of bone mass in this area. In all scenarios, the risk of wrist fracture is the most likely type of fracture. We did not find any statistically significant differences in fracture probability by gender in any situation. The potential for spinal fracture due to lifting heavy objects is quite low while within the spacecraft, but it may pose a risk during EVAs on Mars missions due to the weight of the spacesuit and compromised bone integrity resulting from an extended period in reduced gravity. The risk of spinal fracture due to up to 2-m jumps or falls on the moon appears to pose limited risk, but similar 2-m drops or greater on Mars should be considered more carefully for adverse consequences.

APPENDIX A: CALCULATION OF FRACTURE PROBABILITY FROM FRACTURE RISK INDEX

Davidson *et al.*[26] provided a means of linking estimates of fracture risk index, FRI, to fracture probability, p_{fx}, through the use of logistic regression to

compare the binary condition of actual fractures to non-fractures, with reference to a set of appropriate controls and specified loading events. The logistic regression used in this study results in a sigmoidal curve represented by:

$$p_{\mathrm{fx}} = \frac{1}{(1 + \exp(-1 * (\mathrm{FRI} - \mu) * \phi))} \tag{A1}$$

where μ is the position factor of the curve (the value of FRI where the probability is 0.50) and ϕ is the slope factor (a measure of the steepness of the curve). Ideally, the development of relevant values of μ and ϕ would be derived from data of actual skeletal loading events, in which conditions and outcomes (fracture or no fracture), are well documented. Such data are needed to ensure that the FRI to probability relation is consistent with the methods used in the prediction of FRI. Unfortunately, data of this type are lacking in the literature. Digitizing and post-processing Davidson *et al.*'s data, derived from radial arm fractures in children caused by falls from playground equipment, reveal values of μ and ϕ in the range of 0.58 to 0.6 and 7.5 to 12, respectively. Although not directly applicable to the case of astronaut fractures, these values provide a rational first comparison in evaluating a translation function linking the FRI to estimated fracture probability for astronauts.

To develop the translation function for astronauts without direct loading and fracture data, we must make several assumptions concerning the sigmoidal function parameters, and determine an acceptable fracture threshold range. Several articles in the literature suggest that, at the proximal femur, the fracture threshold (the range when the probability of fracture is not negligible) occurs when the applied load, AL, equals fracture load, FL, within $\pm 1\sigma$ of the bone strength[17,58] or

$$0 < p_{\mathrm{fx}} < 1 \quad \text{when } \mathrm{FL} - \sigma_{\mathrm{FL}} < \mathrm{AL} < \mathrm{FL} + \sigma_{\mathrm{FL}}$$

where p_{fx} is the probability of fracture (a number between 0 and 1) and σ is the standard deviation. For our purposes, this threshold would formally translate to:

$$0 < p_{\mathrm{fx}} < 1 \quad \text{when } 1 - \sigma_{\mathrm{FRI}} < \mathrm{FRI} < 1 + \sigma_{\mathrm{FRI}}$$

$$\sigma_{\mathrm{FRI}=1} = \left[\left(\sigma_{\mathrm{AL}} \frac{1}{\mathrm{FL}} \right)^2 + \left(\sigma_{\mathrm{FL}} \frac{\mathrm{AL}}{2\mathrm{FL}^2} \right)^2 \right]^{1/2} \tag{A2}$$

The threshold of fracture has a mean value of FRI = 1, and the uncertainty of the threshold value is dependent on the standard deviations of AL and FL. Making use of the fact that at FRI = 1, AL = FL, and using the uncertainty of the loading condition and bone strengths, we estimated that $0.135 < \sigma_{\mathrm{FRI}=1} < 0.22$. However, testing of the model using the parameter space imposed by the astronaut data resulted in a standard deviation of the FRI estimates ranging from 0.29 to 0.67. This is due, in part, to the inclusion of other parameter uncertainties and the generally higher mean values of FRI that are calculated. Therefore, to be inclusive of all available data and corresponding uncertainties, the formal estimate of σ at FRI = 1 was adjusted to range from 0.135 to 0.67 in all of the calculations presented in this paper.

To be reasonably confident that the estimated range of μ and ϕ includes the "true" range of μ and ϕ, the following assumptions are made based on the guidance found in the literature:

1. The mean FRI threshold value is 1
2. At $\mathrm{FRI} = 1 + \sigma_{\mathrm{FRI}=1}$, $p_{\mathrm{fx}} = 0.95$ represents the upper limit of the fracture threshold
3. At $\mathrm{FRI} = 1 - \sigma_{\mathrm{FRI}=1}$, $p_{\mathrm{fx}} = 0.05$ represents the lower limit of the fracture threshold

In order to use these assumptions to generate a range of possible ϕ values, the sigmoid equation is first solved for ϕ. This gives:

$$\phi = -1 * \frac{\ln\left(\frac{1}{p_{\mathrm{fx}}} - 1\right)}{(\mathrm{FRI} \pm \sigma_{\mathrm{FRI}=1} - \mu)} \tag{A3}$$

Under our assumptions that the threshold value for FRI = 1, and assuming $\mu = 1$, then the range for ϕ in the threshold region is found to be dependent only on $\sigma_{\mathrm{FRI}=1}$. For the estimated range of $\sigma_{\mathrm{FRI}=1}$, the range of estimated ϕ is found to be $4.4 < \theta < 22$. This approach produces a range on ϕ that is inclusive of the values estimated by Davidson *et al.*[26]

We can again turn to the sigmoid equation to assist in estimating the range of values for μ. Rearranging the sigmoid equation, μ can be calculated as:

$$\mu = \frac{\ln\left(\frac{1}{p_{\mathrm{fx}}} - 1\right)}{\phi} + (\mathrm{FRI} \pm \sigma_{\mathrm{FRI}=1}) \tag{A4}$$

Assuming that the mean FRI = 1 and using the previous calculation, the mean value for ϕ is evaluated as 13.2. Applying the change in p_{fx} and $\sigma_{\mathrm{FRI}=1}$ over the combination of their respective ranges, the range for μ is found to be $0.55 < \mu < 1.45$, which is inclusive of the Davidson *et al.*[26] estimates. The limits on the family of sigmoid curves, as described over the range of μ and ϕ, are illustrated in Fig. A.1. Although additional data would reduce the uncertainty in these calculations, the approach described here reasonably bounds the available knowledge base, makes use of expert opinion in

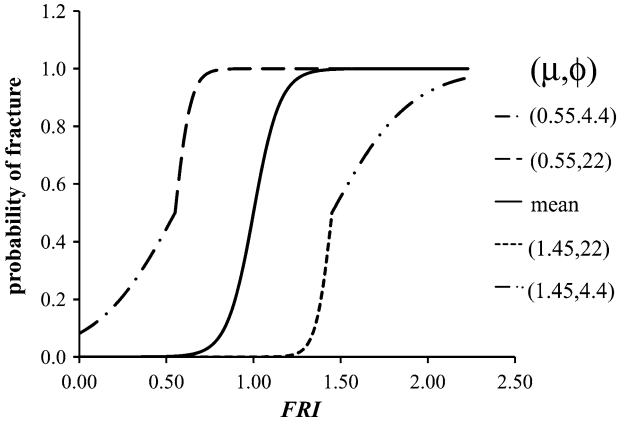

FIGURE A.1. Sigmoid curve family representing the estimated fracture threshold translation function for transforming FRI to probability of fracture. Solid line represents mean value of μ and ϕ, while upper and lower fracture thresholds are shown in dotted lines at specified combinations of (μ, ϕ).

the literature, and provides a consistent means of representing the uncertainty in estimating fracture risk probability.

To implement the sigmoid translation function for FRI to fracture probability in the probabilistic model for fracture:

1. Uniform probability distributions were established over the range of μ and ϕ.
2. At each trial when an FRI value was calculated in the model, the μ and ϕ distributions were randomly sampled.
3. Using the randomly sampled combined values of μ and ϕ, a translation function using the general form of the sigmoid equation was used to estimate the probability of fracture from the FRI value.

Uniform probability distributions are sometimes referred to as "maximum uncertainty" distributions since no value is more probable to occur than any other value within the limits of the distribution. We chose this type of distribution for estimating μ and ϕ due to the lack of knowledge regarding the shape of a representative probability density function and to formally represent the large (epistemic) uncertainty in this area of the model.

APPENDIX B: EQUATIONS FOR BIOMECHANICAL MODEL OF THE HIP AND LUMBAR SPINE

The biomechanical models for dynamic loading shown in Figs. 3b–3d lead to sets of first-order differential equations with unknown time-dependent displacements, x, and velocities, $\dot{x}$. For the case of the hip, the equation of motion is:

$$m_H\ddot{x}_H + b_H\dot{x}_H + k_H x_H = m_F g \tag{B1}$$

where the subscript H refers to the hip, m is the mass of the body, $\ddot{x}$ is the acceleration, k is the spring constant, and b is the damping coefficient. In all cases, the initial displacement is set to zero, and the impact velocity is set to $\sqrt{2gh}$, where h is the distance fallen. In this case, h is defined as the distance between the ground and the hip.

The equations can be more compactly written as matrix equations, in which the unknown displacement x_H is set to x_1 and the unknown velocity, $\dot{x}_1$ to x_2

$$\begin{bmatrix}\dot{x}_1\\ \dot{x}_2\end{bmatrix} = \begin{bmatrix}0 & 1\\ -b/m & -k/m\end{bmatrix}\begin{bmatrix}x_1\\ x_2\end{bmatrix} + \begin{bmatrix}0\\ g\end{bmatrix} \tag{B2}$$

The initial conditions are zero displacement and impact velocity as set by the local gravitational acceleration:

$$\begin{bmatrix}x_1(0)\\ x_2(0)\end{bmatrix} = \begin{bmatrix}0\\ \sqrt{2gh}\end{bmatrix} \tag{B3}$$

Once the system of equations is solved, the ground reaction force, F_{GR}, is found by summing the damping and spring forces that are applied between the body and the ground:

$$F_{GR} = bx_2 + kx_1 \tag{B4}$$

For the femoral fracture model, F_{GR} multiplied by attenuation factors for the fall orientation and active response is the applied load to the bone. In the biomechanical models for the lumbar spine and the wrist, the body is represented as a series of linked masses connected with linear springs and dampers. For the lumbar spine:

$$\begin{aligned}
&m_F\ddot{x}_F + \dot{x}_F b_G + x_F k_G + (x_F - x_{PL})k_L = m_F g\\
&m_{PL}\ddot{x}_{PL} + (\dot{x}_{PL} - \dot{x}_{HAT})b_{LS} + (x_{PL} - x_{HAT})k_{LS}\\
&\quad + (x_{PL} - x_F)k_L = m_{PL} g\\
&m_{HAT}\ddot{x}_{HAT} + (\dot{x}_{HAT} - \dot{x}_{PL})b_{LS}\\
&\quad + (x_{HAT} - x_{PL})k_{LS} = m_{HAT} g
\end{aligned} \tag{B5}$$

When we perform a similar re-definition of the matrix variables by:

$$\begin{aligned}
x_1 &= x_F\\
x_2 &= \dot{x}_1\\
x_3 &= x_{PL}\\
x_4 &= \dot{x}_3\\
x_5 &= x_{HAT}\\
x_6 &= \dot{x}_5
\end{aligned} \tag{B6}$$

then the following matrix equation can be found:

$$\begin{bmatrix} \dot{x}_1 \\ \dot{x}_2 \\ \dot{x}_3 \\ \dot{x}_4 \\ \dot{x}_5 \\ \dot{x}_6 \end{bmatrix} = \begin{bmatrix} 0 & 1 & 0 & 0 & 0 & 0 \\ -(k_G + k_L)/m_F & -b_G/m_F & k_L/m_F & 0 & 0 & 0 \\ 0 & 0 & 0 & 1 & 0 & 0 \\ k_L/m_{PL} & 0 & -(k_L + k_{LS})/m_{PL} & -b_{LS}/m_{PL} & k_{LS}/m_{PL} & b_{LS}/m_{PL} \\ 0 & 0 & 0 & 0 & 0 & 1 \\ 0 & 0 & k_{LS}/m_{HAT} & b_{LS}/m_{HAT} & -k_{LS}/m_{HAT} & -b_{LS}/m_{HAT} \end{bmatrix} \cdot \begin{bmatrix} x_1 \\ x_2 \\ x_3 \\ x_4 \\ x_5 \\ x_6 \end{bmatrix} + \begin{bmatrix} 0 \\ g \\ 0 \\ g \\ 0 \\ g \end{bmatrix} \tag{B7}$$

with initial conditions:

$$\begin{bmatrix} x_1(0) \\ x_2(0) \\ x_3(0) \\ x_4(0) \\ x_5(0) \\ x_6(0) \end{bmatrix} = \begin{bmatrix} 0 \\ \sqrt{2gh} \\ 0 \\ \sqrt{2gh} \\ 0 \\ \sqrt{2gh} \end{bmatrix} \tag{B8}$$

Similar to the hip model, the ground reaction force, F_{GR}, and the force on the lumbar spine, F_{LS}, is given by:

$$F_{GR} = b_G x_2 + k_G x_1$$

$$F_{LS} = b_{LS}(x_6 - x_4) + k_{LS}(x_5 - x_3)$$

The force on the lumbar spine is equivalent to the applied load to the spine, which was then used in the spinal fracture model.

ACKNOWLEDGMENTS

The BFxRM is a component of the NASA Integrated Medical Model Task under the NASA Exploration Medicine Capabilities Element. We gratefully acknowledge support from the NASA Human Research Program, critical input from Dr. Jean Sibonga, and substantial assistance in portions of the model development from Christina Sulkowski and Kelley Ruehl.

REFERENCES

[1]Amin, S. BMD data for the ultradistal radius. Personal communication, 2008.
[2]Anthropometric Source Book. Volume I: Anthropometry for Designers. Yellow Springs, OH: Webb Associates, 1978.
[3]Anthropometry and mass distribution for human analogues. Volume I: Military aviators. Anthropology Research Project. AAMRL-TR-88-010. 21988, 1978.
[4]Arampatzis, A., G. P. Bruggemann, and G. M. Klapsing. Leg stiffness and mechanical energetic processes during jumping on a sprung surface. *Med. Sci. Sports Exerc.* 33:923–931, 2001.
[5]Arampatzis, A., G. P. Bruggemann, and V. Metzler. The effect of speed on leg stiffness and joint kinetics in human running. *J. Biomech.* 32:1349–1353, 1999.
[6]Arampatzis, A., F. Schade, M. Walsh, and G. P. Bruggemann. Influence of leg stiffness and its effect on myodynamic jumping performance. *J. Electromyogr. Kinesiol.* 11:355–364, 2001.
[7]Arampatzis, A., S. Stafilidis, G. Morey-Klapsing, and G. P. Bruggemann. Interaction of the human body and surfaces of different stiffness during drop jumps. *Med. Sci. Sports Exerc.* 36:451–459, 2004.
[8]Beck, T. J., C. B. Ruff, K. E. Warden, W. W. Scott, Jr., and G. U. Rao. Predicting femoral neck strength from bone mineral data. A structural approach. *Invest. Radiol.* 25:6–18, 1990.
[9]Bensch, F. V., M. J. Kiuru, M. P. Koivikko, and S. K. Koskinen. Spine fractures in falling accidents: analysis of multidetector CT findings. *Eur. Radiol.* 14:618–624, 2004.
[10]Biggemann, M., D. Hilweg, S. Seidel, M. Horst, and P. Brinckmann. Risk of vertebral insufficiency fractures in relation to compressive strength predicted by quantitative computed tomography. *Eur. J. Radiol.* 13:6–10, 1991.
[11]Bouxsein, M. L., L. J. Melton, III, B. L. Riggs, J. Muller, E. J. Atkinson, A. L. Oberg, R. A. Robb, J. J. Camp, P. A. Rouleau, C. H. McCollough, and S. Khosla. Age- and sex-specific differences in the factor of risk for vertebral fracture: a population-based study using QCT. *J. Bone Miner. Res.* 21:1475–1482, 2006.
[12]Branke, J., K. Deb, K. Mitetinen, and R. Slowinski. Multiobjective Optimization: Interactive and Evolutionary Approaches. Springer, 2008.
[13]Brinckmann, P., M. Biggemann, and D. Hilweg. Prediction of the compressive strength of human lumbar vertebrae. *Spine* 14:606–610, 1989.
[14]Carpenter, R. D., G. S. Beaupre, T. F. Lang, E. S. Orwoll, and D. R. Carter. New QCT analysis approach shows the importance of fall orientation on femoral neck strength. *J. Bone Miner. Res.* 20:1533–1542, 2005.
[15]Chaffin, D. B. A computerized biomechanical model-development of and use in studying gross body actions. *J. Biomech.* 2:429–441, 1969.

[16]Chaffin, D. B., and W. H. Baker. A biomechanical model for analysis of symmetric sagittal plane lifting. *AIIE Trans*. 2:16–27, 1970.
[17]Cheng, X. G., G. Lowet, S. Boonen, P. H. Nicholson, P. Brys, J. Nijs, and J. Dequeker. Assessment of the strength of proximal femur in vitro: relationship to femoral bone mineral density and femoral geometry. *Bone* 20:213–218, 1997.
[18]Cheng, X. G., G. Lowet, S. Boonen, P. H. F. Nicholson, G. van der Perre, and J. Dequeker. Prediction of vertebral and femoral strength in vitro by bone mineral density measured at different skeletal sites. *J. Bone Miner. Res*. 13:1439–1443, 1998.
[19]Chi, K. J., and D. Schmitt. Mechanical energy and effective foot mass during impact loading of walking and running. *J. Biomech*. 38:1387–1395, 2005.
[20]Chiu, J., and S. N. Robinovitch. Prediction of upper extremity impact forces during falls on the outstretched hand. *J. Biomech*. 31:1169–1176, 1998.
[21]Chou, P. H., Y. L. Chou, C. J. Lin, F. C. Su, S. Z. Lou, C. F. Lin, and G. F. Huang. Effect of elbow flexion on upper extremity impact forces during a fall. *Clin. Biomech*. 16(10):888–894, 2001.
[22]Crawford, R. P., C. E. Cann, and T. M. Keaveny. Finite element models predict in vitro vertebral body compressive strength better than quantitative computed tomography. *Bone* 33:744–750, 2003.
[23]Crawford, R. P., and T. M. Keaveny. Relationship between axial and bending behaviors of the human thoracolumbar vertebra. *Spine* 29:2248–2255, 2004.
[24]Cummings, S. R., D. B. Karpf, F. Harris, H. K. Genant, K. Ensrud, A. Z. LaCroix, and D. M. Black. Improvement in spine bone density and reduction in risk of vertebral fractures during treatment with antiresorptive drugs. *Am. J. Med*. 112:281–289, 2002.
[25]Dai, L. The relationship between vertebral body deformity and disc degeneration in lumbar spine of the senile. *Eur. Spine J*. 7:40–44, 1998.
[26]Davidson, P. L., D. J. Chalmers, and S. C. Stephenson. Prediction of distal radius fracture in children, using a biomechanical impact model and case–control data on playground free falls. *J. Biomech*. 39(3):503–509, 2006.
[27]DeGoede, K. M., and J. A. Ashton-Miller. Fall arrest strategy affects peak hand impact force in a forward fall. *J. Biomech*. 35:843–848, 2002.
[28]Demetriades, D., J. Murray, C. Brown, G. Velmahos, A. Salim, K. Alo, and P. Rhee. High-level falls: type and severity of injuries and survival outcome according to age. *J. Trauma* 58:342–345, 2005.
[29]Duan, Y., E. Seeman, and C. H. Turner. The biomechanical basis of vertebral body fragility in men and women. *J. Bone Miner. Res*. 16(12):2276–2283, 2001.
[30]Duma, S. M., A. R. Kemper, D. M. McNeely, P. G. Brolinson, and F. Matsuoka. Biomechanical response of the lumbar spine in dynamic compression. *Biomed. Sci. Instrum*. 42:476–481, 2006.
[31]Ebbesen, E. N., J. S. Thomsen, H. Beck-Nielsen, H. J. Nepper-Rasmussen, and L. Mosekilde. Lumbar vertebral body compressive strength evaluated by dual-energy X-ray absorptiometry, quantitative computed tomography, and ashing. *Bone* 25:713–724, 1999.
[32]Ebong, W. W. Falls from trees. *Trop. Geogr. Med*. 30:63–67, 1978.
[33]Eckstein, F., M. Fischbeck, V. Kuhn, T. M. Link, M. Priemel, and E. M. Lochmuller. Determinants and heterogeneity thoracolumbar spine of mechanical competence throughout the of elderly women and men. *Bone* 35:364–374, 2004.
[34]Edmondston, S. J., K. P. Singer, R. E. Day, R. I. Price, and P. D. Breidahl. Ex vivo estimation of thoracolumbar vertebral body compressive strength: The relative contributions of bone densitometry and vertebral morphometry. *Osteoporos. Int*. 7:142–148, 1997.
[35]Engelund, W. C., R. W. Powell, and R. H. Tolson. Atmospheric modeling challenges and measurement requirements for Mars entry, descent and landing. #9025. Third International Workshop on the Mars Atmosphere: Modeling and Observations. Mars atmosphere: Modeling and observations, 11/2008.
[36]Eswaran, S. K., A. Guta, M. F. Adams, and T. M. Keaveny. Cortical and trabecular load sharing in the human vertebral body. *J. Bone Miner. Res*. 21:307–314, 2006.
[37]EVA Design Requirements and Considerations. JSC-39117. Houston, TX: NASA Johnson Space Center, 2004.
[38]Extravehicular (EVA) Hardware Generic Design Requirements Document. JSC-26626. Houston, TX: NASA Johnson Space Center, 1994.
[39]Farley, C. T., and D. C. Morgenroth. Leg stiffness primarily depends on ankle stiffness during human hopping. *J. Biomech*. 32:267–273, 1999.
[40]Ferris, D. P., and C. T. Farley. Interaction of leg stiffness and surface stiffness during human hopping. *J. Appl. Physiol*. 82:15–22, 1997.
[41]Ferris, D. P., K. L. Liang, and C. T. Farley. Runners adjust leg stiffness for their first step on a new running surface. *J. Biomech*. 32:787–794, 1999.
[42]Fiolkowski, P., M. Bishop, D. Brunt, and B. Williams. Plantar feedback contributes to the regulation of leg stiffness. *Clin. Biomech*. 20:952–958, 2005.
[43]Ford, C. M., T. M. Keaveny, and W. C. Hayes. The effect of impact direction on the structural capacity of the proximal femur during falls. *J. Bone Miner. Res*. 11:377–383, 1996.
[44]Garnier, K. B., R. Dumas, C. Rumelhart, and M. E. Arlot. Mechanical characterization in shear of human femoral cancellous bone: torsion and shear tests. *Med. Eng. Phys*. 21:641–649, 1999.
[45]George, W. T., and D. Vashishth. Susceptibility of aging human bone to mixed-mode fracture increases bone fragility. *Bone* 38:105–111, 2006.
[46]Gomez-Benito, M. J., J. M. Garcia-Aznar, and M. Doblare. Finite element prediction of proximal femoral fracture patterns under different loads. *J. Biomech. Eng*. 127:9–14, 2005.
[47]Goodacre, S., M. Than, E. C. Goyder, and A. P. Joseph. Can the distance fallen predict serious injury after a fall from a height? *J. Trauma* 46:1055–1058, 1999.
[48]Goonetilleke, U. K. Injuries caused by falls from heights. *Med. Sci. Law* 20:262–275, 1980.
[49]Granata, K. P., D. A. Padua, and S. E. Wilson. Gender differences in active musculoskeletal stiffness. Part II. Quantification of leg stiffness during functional hopping tasks. *J. Electromyogr. Kinesiol*. 12:127–135, 2002.
[50]Greer, W., R. Smith, and A. J. Shipman. A multi-exponential model of postmenopausal decline in vertebral bone mineral density—a new approach to the BMD reference range. *J. Clin. Densitom*. 6:113–124, 2003.
[51]Hayes, W. C., and E. R. Myers. Biomechanical considerations of hip and spine fractures in osteoporotic bone.

In: Proceedings AAOS Instructional Lectures, edited by D. Springfield. *Instr. Course Lect.* 46:431–438, 1997.
[52]Homminga, J., B. Van-Rietbergen, E. M. Lochmuller, H. Weinans, F. Eckstein, and R. Huiskes. The osteoporotic vertebral structure is well adapted to the loads of daily life, but not to infrequent "error" loads. *Bone* 34:510–516, 2004.
[53]Hsiao, E. T., and S. N. Robinovitch. Common protective movements govern unexpected falls from standing height. *J. Biomech.* 31:1–9, 1998.
[54]Hudelmaier, M., V. Kuhn, E. M. Lochmuller, H. Well, M. Priemel, T. M. Link, and F. Eckstein. Can geometry-based parameters from pQCT and material parameters from quantitative ultrasound (QUS) improve the prediction of radial bone strength over that by bone mass (DXA)? *Osteoporos. Int.* 15:375–381, 2004.
[55]Hui, S. L., C. W. Slemenda, and C. C. Johnston. Age and bone mass as predictors of fracture in a prospective study. *J. Clin. Invest.* 81:1804–1809, 1988.
[56]Izambert, O., D. Mitton, M. Thourot, and F. Lavaste. Dynamic stiffness and damping of human intervertebral disc using axial oscillatory displacement under a free mass system. *Eur. Spine J.* 12:562–566, 2003.
[57]Kanis, J. A., O. Johnell, A. Oden, B. Jonsson, C. De Laet, and A. Dawson. Risk of hip fracture according to the World Health Organization criteria for osteopenia and osteoporosis. *Bone* 27:585–590, 2000.
[58]Kannus, P., J. Parkkari, and J. Poutala. Comparison of force attenuation properties of four different hip protectors under simulated falling conditions in the elderly: an in vitro biomechanical study. *Bone* 25:229–235, 1999.
[59]Keyak, J. H., A. K. Koyama, A. LeBlanc, Y. Lu, and T. F. Lang. Reduction in proximal femoral strength due to long-duration spaceflight. *Bone* 44:449–453, 2009.
[60]Keyak, J. H., H. B. Skinner, and J. A. Fleming. Effect of force direction on femoral fracture load for two types of loading conditions. *J. Orthop. Res.* 19:539–544, 2001.
[61]Kim, K. J., A. M. Alian, W. S. Morris, and Y. H. Lee. Shock attenuation of various protective devices for prevention of fall-related injuries of the forearm/hand complex. *Am. J. Sports Med.* 34:637–643, 2006.
[62]Kong, W., K. Kash, and C. Lee. Biomechanical modeling of paratrooper landings. AIAA-2001-2029, 2001.
[63]Kukla, C., C. Gaebler, R. W. Pichl, R. Prokesch, G. Heinze, and T. Heinz. Predictive geometric factors in a standardized model of femoral neck fracture. Experimental study of cadaveric human femurs. *Injury* 33:427–433, 2002.
[64]Lafortune, M. A., M. J. Lake, and E. M. Hennig. Differential shock transmission response of the human body to impact severity and lower limb posture. *J. Biomech.* 29:1531–1537, 1996.
[65]Lang, T. F., A. D. LeBlanc, H. J. Evans, and Y. Lu. Adaptation of the proximal femur to skeletal reloading after long-duration spaceflight. *J. Bone Miner. Res.* 21:1224–1230, 2006.
[66]Lapostolle, F., C. Gere, S. W. Borron, T. Petrovic, F. Dallemagne, A. Beruben, C. Lapandry, and N. Adnet. Prognostic factors in victims of falls from height. *Crit. Care Med.* 33:1239–1242, 2005.
[67]LeBlanc, A., C. Lin, L. Shackelford, V. Sinitsyn, H. Evans, O. Belichenko, B. Schenkman, I. Kozlovskaya, V. Oganov, A. Bakulin, T. Hedrick, and D. Feeback. Muscle volume, MRI relaxation times (T2), and body composition after spaceflight. *J. Appl. Physiol.* 89:2158–2164, 2000.
[68]LeBlanc, A., V. Schneider, L. Shackelford, S. West, V. Oganov, A. Bakulin, and L. Voronin. Bone mineral and lean tissue loss after long duration space flight. *J. Musculoskelet. Neuronal Interact.* 1:157–160, 2000.
[69]Licata, A. Bone density vs. bone quality: What's a clinician to do? *Cleve. Clin. J. Med.* 76:331–336, 2009.
[70]Lindsey, D. P., M. J. Kim, M. Hannibal, and T. F. Alamin. The monotonic and fatigue properties of osteoporotic thoracic vertebral bodies. *Spine* 30:645–649, 2005.
[71]Lo, J., G. N. Mccabe, K. M. DeGoede, H. Okuizumi, and J. A. Ashton-Miller. On reducing hand impact force in forward falls: results of a brief intervention in young males. *Clin. Biomech.* 18:730–736, 2003.
[72]Lowenstein, S. R., M. Yaron, R. Carrero, D. Devereux, and L. M. Jacobs. Vertical trauma: injuries to patients who fall and land on their feet. *Ann. Emerg. Med.* 18:161–165, 1989.
[73]Lubahn, J., R. Englund, G. Trinidad, J. Lyons, D. Ivance, and F. L. Buczek. Adequacy of laboratory simulation of in-line skater falls. *J. Hand Surg.* 30:283–288, 2005.
[74]MacNeil, J. A., and S. K. Boyd. Load distribution and the predictive power of morphological indices in the distal radius and tibia by high resolution peripheral quantitative computed tomography. *Bone* 41:129–137, 2007.
[75]Maimoun, L., C. Fattal, J. P. Micallef, E. Peruchon, and P. Rabischong. Bone loss in spinal cord-injured patients: from physiopathology to therapy. *Spinal Cord* 44:203–210, 2006.
[76]Man-Systems Integration Standards. Volume I. Boeing Aerospace Company. NASA STD-3000, 1995.
[77]Marras, W. S., and C. M. Sommerich. A three-dimensional motion model of loads on the lumbar spine. I. Model structure. *Hum. Factors* 33:123–137, 1991.
[78]McNair, P. J., and P. Prasad. Normative data of vertical ground reaction forces during landing from a jump. *J. Sci. Med. Sport* 2:86–88, 1999.
[79]Melton, III, L. J., S. Khosla, S. J. Achenbach, M. K. O'Connor, W. M. O'fallon, and B. L. Riggs. Effects of body size and skeletal site on the estimated prevalence of osteoporosis in women and men. *Osteoporos. Int.* 11:977–983, 2000.
[80]Minaire, P., P. Neunier, C. Edouard, J. Bernard, P. Courpron, and J. Bourret. Quantitative histological data on disuse osteoporosis: comparison with biological data. *Calcif. Tissue Res.* 17:57–73, 1974.
[81]Mizrahi, J., M. J. Silva, and W. C. Hayes. Finite element stress analysis of simulated metastatic lesions in the lumbar vertebral body. *J. Biomed. Eng.* 14:467–475, 1992.
[82]Mizrahi, J., M. J. Silva, T. M. Keaveny, W. T. Edwards, and W. C. Hayes. Finite-element stress analysis of the normal and osteoporotic lumbar vertebral body. *Spine* 18:2088–2096, 1993.
[83]Mizrahi, J., and Z. Susak. In vivo elastic and damping response of the human leg to impact forces. *J. Biomech. Eng.* 104:63–66, 1982.
[84]Moga, P. J., M. Erig, D. B. Chaffin, and M. A. Nussbaum. Torso muscle moment arms at intervertebral levels T10 through L5 from CT scans on eleven male and eight female subjects. *Spine* 18:2305–2309, 1993.
[85]Moritz, C. T., and C. T. Farley. Passive dynamics change leg mechanics for an unexpected surface during human hopping. *J. Appl. Physiol.* 97:1313–1322, 2004.

[86]Moro, M., A. T. Hecker, M. L. Bouxsein, and E. R. Myers. Failure load of thoracic vertebrae correlates with lumbar bone mineral density measured by DXA. *Calcif. Tissue Int*. 56:206–209, 1995.
[87]Muller, M. E., C. E. Webber, and J. D. Adachi. Hormone replacement therapy improves distal radius bone structure by endocortical mineral deposition. *Can. J. Physiol. Pharmacol*. 81:952–958, 2003.
[88]Muller, M. E., C. E. Webber, and M. L. Bouxsein. Predicting the failure load of the distal radius. *Osteoporos. Int*. 14:345–352, 2003.
[89]Mussolino, M. E., A. C. Looker, and E. S. Orwoll. Jogging and bone mineral density in men: results from NHANES III. *Am. J. Public Health* 91:1056–1059, 2001.
[90]Myers, E. R., and S. E. Wilson. Biomechanics of osteoporosis and vertebral fracture. *Spine* 22:25S–31S, 1997.
[91]NASA Longitudinal Study of Astronaut Health. http://lsda.jsc.nasa.gov/docs/research/research_detail.cfm?experiment_type_code=23&researchtype=current, 2009.
[92]NASA Space flight human system standard. Volume 1: Crew health. NASA-STD-3001. National Aeronautics and Space Administration, 2007.
[93]Nelson, E. S., B. Lowenstein, A. Licata, and J. G. Myers. Interpreting population studies of falls from height. NASA Technical Memorandum, 2009 (submitted).
[94]Nguyen-Thanh, Q., C. Tresallet, O. Langeron, B. Riou, and F. Menegaux. Polytrauma is more severe after a free fall from a height than after a motor vehicle accident. *Ann. Chir*. 128:526–529, 2003.
[95]Nicholson, P. H., X. G. Cheng, G. Lowet, S. Boonen, M. W. Davie, J. Dequeker, and G. Van der Perre. Structural and material mechanical properties of human vertebral cancellous bone. *Med. Eng. Phys*. 19:729–737, 1997.
[96]Ochia, R. S., and R. P. Ching. Internal pressure measurements during burst fracture formation in human lumbar vertebrae. *Spine* 27:1160–1167, 2002.
[97]Ochia, R. S., A. F. Tencer, and R. P. Ching. Effect of loading rate on endplate and vertebral body strength in human lumbar vertebrae. *J. Biomech*. 36:1875–1881, 2003.
[98]Ong, A., P. T. C. Iau, A. W. Yeo, M. P. Koh, and G. K. K. Lau. Victims of falls from a height surviving to hospital admission in two Singapore hospitals. *Med. Sci. Law* 44:201–206, 2004.
[99]Ott, S. Osteoporosis and bone physiology. http://courses.washington.edu/bonephys/opbmdtz.html, 11-25-2006.
[100]Padua, D. A., C. R. Carcia, B. L. Arnold, and K. P. Granata. Gender differences in leg stiffness and stiffness recruitment strategy during two-legged hopping. *J. Mot. Behav*. 37:111–125, 2005.
[101]Pinilla, T. P., K. C. Boardman, M. L. Bouxsein, E. R. Myers, and W. C. Hayes. Impact direction from a fall influences the failure load of the proximal femur as much as age-related bone loss. *Calcif. Tissue Int*. 58:231–235, 1996.
[102]Pistoia, W., B. Van Rietbergen, E. M. Lochmuller, C. A. Lill, F. Eckstein, and P. Ruegsegger. Estimation of distal radius failure load with micro-finite element analysis models based on three-dimensional peripheral quantitative computed tomography images. *Bone* 30:842–848, 2002.
[103]Polikeit, A., L. P. Nolte, and S. J. Ferguson. Simulated influence of osteoporosis and disc degeneration on the load transfer in a lumbar functional spinal unit. *J. Biomech*. 37:1061–1069, 2004.
[104]Prasad, P., and A. I. King. An experimentally validated dynamic model of the spine. *J. Appl. Mech. Trans. ASME* 41:546–550, 1974.
[105]Renau, A., J. Farrerons, B. Yoldi, J. Gil, I. Proubasta, J. Llauger, J. G. Olivan, and J. Planell. Yield point in prediction of compressive behavior of lumbar vertebral body by dual-energy X-ray absorptiometry. *J. Clin. Densitom*. 7:382–389, 2004.
[106]Reynolds, B. M., N. A. Balsano, and F. X. Reynolds. Falls from heights: a surgical experience of 200 consecutive cases. *Ann. Surg*. 174:304–308, 1971.
[107]Richter, D., M. P. Hahn, P. A. Ostermann, A. Ekkernkamp, and G. Muhr. Vertical deceleration injuries: a comparative study of the injury patterns of 101 patients after accidental and intentional high falls. *Injury* 27:655–659, 1996.
[108]Riggs, B. L., L. J. Melton, III, R. A. Robb, J. J. Camp, E. J. Atkinson, A. L. Oberg, P. A. Rouleau, C. H. McCollough, S. Khosla, and M. L. Bouxsein. Population-based analysis of the relationship of whole bone strength indices and fall-related loads to age- and sex-specific patterns of hip and wrist fractures. *J. Bone Miner. Res*. 21:315–323, 2006.
[109]Robinovitch, S. N., W. C. Hayes, and T. A. McMahon. Distribution of contact force during impact to the hip. *Ann. Biomed. Eng*. 25:499–508, 1997.
[110]Sabick, M. B., J. G. Hay, V. K. Goel, and S. A. Banks. Active responses decrease impact forces at the hip and shoulder in falls to the side. *J. Biomech*. 32:993–998, 1999.
[111]Scalea, T., A. Goldstein, T. Phillips, S. J. Sclafani, T. Panetta, J. McAuley, and G. Shaftan. An analysis of 161 falls from a height: the 'jumper syndrome'. *J. Trauma* 26:706–712, 1986.
[112]Schultz, A., G. B. Andersson, R. Ortengren, R. Bjork, and M. Nordin. Analysis and quantitative myoelectric measurements of loads on the lumbar spine when holding weights in standing postures. *Spine* 7:390–397, 1982.
[113]Seegmiller, J. G., and S. T. McCaw. Ground reaction forces among gymnasts and recreational athletes in drop landings. *J. Athl. Train*. 38:311–314, 2003.
[114]Shackelford, L. C., A. D. LeBlanc, T. B. Driscoll, H. J. Evans, N. J. Rianon, S. M. Smith, E. Spector, D. L. Feeback, and D. Lai. Resistance exercise as a countermeasure to disuse-induced bone loss. *J. Appl. Physiol*. 97:119–129, 2004.
[115]Sibonga, J. Compilation of pre and post flight Astronaut aBMD. Personal communication, 2006.
[116]Sibonga, J. D., H. J. Evans, H. G. Sung, E. R. Spector, T. F. Lang, V. S. Oganov, A. V. Bakulin, L. C. Shackelford, and A. D. LeBlanc. Recovery of spaceflight-induced bone loss: Bone mineral density after long-duration missions as fitted with an exponential function. *Bone* 41:973–978, 2007.
[117]Singer, K., S. Edmondston, R. Day, P. Breidahl, and R. Price. Prediction of thoracic and lumbar vertebral body compressive strength—correlations with bone mineral density and vertebral region. *Bone* 17:167–174, 1995.
[118]Snyder, R. G. Human tolerances to extreme impacts in free fall. *Aerosp. Med*. 34:695–709, 1963.
[119]Song, Y., M. A. Liebschner, and G. H. Gunaratne. A study of age-related architectural changes that are most damaging to bones. *Biophys. J*. 87:3642–3647, 2004.
[120]Sran, M. M., K. M. Khan, Q. A. Zhu, H. A. McKay, and T. R. Oxland. Failure characteristics of the thoracic spine with a posteroanterior load: Investigating the safety of spinal mobilization. *Spine* 29:2382–2388, 2004.
[121]Staebler, M. P., D. C. Moore, E. Akelman, A. P. C. Weiss, P. D. Fadale, and J. J. Crisco. The effect of wrist guards on bone strain in the distal forearm. *Am. J. Sports Med*. 27:500–506, 1999.

[122]Sugita, H., M. Oka, J. Toguchida, T. Nakamura, T. Ueo, and T. Hayami. Anisotropy of osteoporotic cancellous bone. *Bone* 24:513–516, 1999.
[123]Taylor, D., E. Casolari, and C. Bignardi. Predicting stress fractures using a probabilistic model of damage, repair and adaptation. *J. Orthop. Res.* 22:487–494, 2004.
[124]Thomas, K. S., and H. J. McMann. US Spacesuits. Springer-Verlag, 2005.
[125]Turk, E. E., and M. Tsokos. Pathologic features of fatal falls from height. *Am. J. Forensic Med. Pathol.* 25:194–199, 2004.
[126]Turner, C. H. Bone strength: current concepts. *Ann. N. Y. Acad. Sci.* 1068:429–446, 2006.
[127]Turner, C. H., T. Wang, and D. B. Burr. Shear strength and fatigue properties of human cortical bone determined from pure shear tests. *Calcif. Tissue Int.* 69:373–378, 2001.
[128]van den Kroonenberg, A. J., W. C. Hayes, and T. A. McMahon. Hip impact velocities and body configurations for voluntary falls from standing height. *J. Biomech.* 29:807–811, 1996.
[129]Velmahos, G. C., D. Demetriades, D. Theodorou, E. E. Cornwell, H. Belzberg, J. Asensio, J. Murray, and T. V. Berne. Patterns of injury in victims of urban free-falls. *World J. Surg.* 21:816–821, 1997.
[130]Velmahos, G. C., K. Spaniolas, H. B. Alam, M. de Moya, A. Gervasini, L. Petrovick, and A. K. Conn. Falls from height: spine, spine, spine!. *J. Am. Coll. Surg.* 203:605–611, 2006.
[131]Wang, Q., J. W. Teo, A. Ghasem-Zadeh, and E. Seeman. Women and men with hip fractures have a longer femoral neck moment arm and greater impact load in a sideways fall. *Osteoporos. Int.* 20:1151–1156, 2009.
[132]Weilemann, Y., M. J. Thali, B. P. Kneubuehl, and S. A. Bolliger. Correlation between skeletal trauma and energy in falls from great height detected by post-mortem multi-slice computed tomography (MSCT). *Forensic Sci. Int.* 180:81–85, 2008.
[133]Wilcox, R. K., D. J. Allen, R. M. Hall, D. Limb, D. C. Barton, and R. A. Dickson. A dynamic investigation of the burst fracture process using a combined experimental and finite element approach. *Eur. Spine J.* 13:481–488, 2004.
[134]Wirbel, R. J., A. Olinger, M. Karst, and W. E. Mutschler. Treatment of severe injuries caused by attempted suicide: Pattern of injury and influence of the psychiatric disorder on the postoperative course. *Eur. J. Surg.* 164:109–113, 1998.
[135]Wu, C., D. Hans, Y. He, B. Fan, C. F. Njeh, P. Augat, J. Richards, and H. K. Genant. Prediction of bone strength of distal forearm using radius bone mineral density and phalangeal speed of sound. *Bone* 26:529–533, 2000.
[136]Yagmur, Y., C. Guloglu, M. Aldemir, and M. Orak. Falls from flat-roofed houses: a surgical experience of 1643 patients. *Injury* 35:425–428, 2004.
[137]Yoganandan, N., A. Sances, Jr., D. J. Maiman, J. B. Myklebust, P. Pech, and S. J. Larson. Experimental spinal injuries with vertical impact. *Spine* 11(9):855–860, 1986.